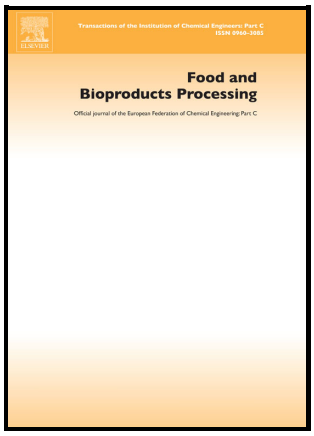

The use of a microhydrodynamic model, kinetic analysis and optimization tools for the development of corn starch nanosuspensions via wet-stirred media milling

María Gabriela Bordón, Lucía López-Vidal, Marcela L Martínez, Santiago D. Palma, Pablo D. Ribotta

PII: S0960-3085(24)00209-8

DOI: https://doi.org/10.1016/j.fbp.2024.10.010

Reference: FBP1898

To appear in: *Food and Bioproducts Processing*

Received date: 20 July 2024
Revised date: 10 October 2024
Accepted date: 12 October 2024

Please cite this article as: María Gabriela Bordón, Lucía López-Vidal, Marcela L Martínez, Santiago D. Palma and Pablo D. Ribotta, The use of a microhydrodynamic model, kinetic analysis and optimization tools for the development of corn starch nanosuspensions via wet-stirred media milling, *Food and Bioproducts Processing,* (2024) doi:https://doi.org/10.1016/j.fbp.2024.10.010

The use of a microhydrodynamic model, kinetic analysis and optimization tools for the development of corn starch nanosuspensions via wet-stirred media milling

Bordón, María Gabriela[1,2*]; López-Vidal, Lucía[4]; Martínez, Marcela L[2,3].; Palma, Santiago D.[4]; Ribotta, Pablo D.[1,2]

[1] Instituto de Ciencia y Tecnología de Alimentos Córdoba (ICYTAC-CONICET, UNC), Córdoba, Argentina
[2] Departamento de Química Industrial y Aplicada (FCEFyN, UNC), Córdoba, Argentina
[3] Instituto Multidisciplinario de Biología Vegetal (IMBIV-CONICET, UNC), Córdoba, Argentina
[4] Unidad de Investigación y Desarrollo en Tecnología Farmacéutica (UNITEFA-CONICET, UNC), Córdoba, Argentina

*Corresponding author: María Gabriela Bordón (maria.gabriela.bordon@mi.unc.edu.ar). ICYTAC, CONICET-UNC, Argentina.

E-mail addresses: l.lopezvidal@unc.edu.ar (Lucía López-Vidal); marcela.martinez@unc.edu.ar (Marcela L. Martínez); sdpalma@unc.edu.ar (Santiago D. Palma); pdribotta@unc.edu.ar (Pablo D. Ribotta).

Abstract.

Starch micro and nanoparticles have emerged as popular stabilizers in food and pharmaceutical formulations. Wet-stirred media milling (WSMM) to develop such particles has not been widely reported, in contrast to chemical hydrolysis. Therefore, this contribution aimed to analyze the effects of: 1) Sodium dodecyl sulfate (SDS) and post-milling operations on the stability of starch nanosuspensions; 2) the bead diameter (d_b) (0.15, 0.50 mm) and starch concentration (c_S) (1, 3.5, 7% w/v) on the type and stability of nanosuspensions, breakage kinetics and microhydrodynamic parameters; 3) spray-drying of nanosuspensions on the structural changes and redispersion of powders. Stable nanosuspensions with an average size of 161±5 nm could be obtained, from an initial size of 14.08±0.08 μm. The use of SDS as a stabilizer prevented aggregation during milling and allowed the formation of amylose-SDS complexes, supported by DSC and X-ray techniques. The microhydrodynamic analysis showed that increasing c_S decreased the compression forces applied to particles. Moreover, the intensity of collisions was improved with a larger d_b. Spray-dried nanosuspensions formulated with a c_S of 7% (w/v), different SDS concentrations (0, 0.07 and 1% w/v), and a d_b of 0.15 mm were analyzed. Submicron particles could only be obtained with 1% (w/v) of SDS: from 366 to 271 nm after milling and spray-drying, respectively. Under these conditions, the granules were fully fragmented, which was confirmed by X-ray and TEM techniques. These results showed that WSMM could be implemented as a solvent-free methodology to obtain biopolymer-based nanoparticles.

Graphical abstract

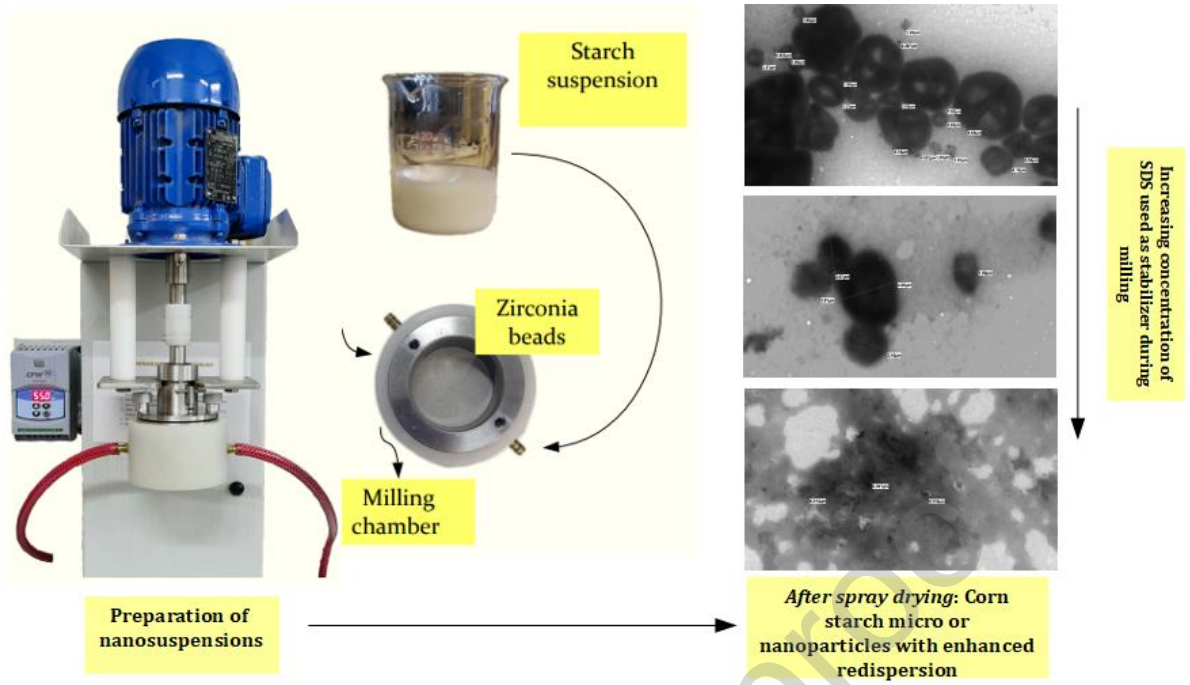

Keywords: corn starch; micro and nanoparticles; wet-stirred media milling; microhydrodynamic analysis; kinetic analysis; optimization.

Abbreviations

a, average frequency of starch particle compressions (Hz).

c, volumetric bead loading in the milling chamber (-).

c_S, starch concentration (%, w/v).

d_b, bead diameter (m).

d_i, individual desirability (-).

d_{50}, particle median diameter (m).

d_{lim}, limiting value of the particle size (m).

D, rotor diameter (m).

D_G, global desirability function (-).

E, energy required for new area creation (J).

F, milling intensity factor (-).

F_b^n, average maximum normal force during the collision of two identical elastic beads (N).

K, coefficient obtained from an empirical correlation (-).

K_i, consistency index ($Pa.s^n$).

n, flow index (-).

P, power applied by the mill motor per unit volume ($W.m^{-3}$).

P', power consumed for new area creation (W).

P_0, power consumed in the absence of grinding media and suspension, per unit volume ($W.m^{-3}$).

P_w, power applied by the mill stirrer per unit volume ($W.m^{-3}$).

P_{ht}, power consumed during the stirring of suspensions in the absence of grinding media, per unit volume ($W.m^{-3}$).

PDI, polydispersity index (-).

Re, Reynolds number (-).

Re_Θ, bead Reynolds number based on granular temperature (-).

R_{diss}, dissipation coefficient (drag coefficient) of the beads (-).

R_{diss0}, dissipation coefficient when the relative motion of the bead-liquid is absent (-).

SSR, size reduction rate ($m.s^{-1}$).

T_0, onset temperature (°C).

T_p, peak temperature (°C).

T_e, endset temperature (°C).

V_C, filled volume in the milling chamber (m^{-3}).

Y *, reduced elastic modulus for the bead-particle contact (Pa).

Y_p, particle's Young modulus (Pa).

Y_b, beads' Young modulus (Pa).

Z, particle size (μm or m, depending on the application).

Greek symbols

α_b^n, radius of the contact circle formed at the contact between two beads (m).

β, empirical coefficient of the Rittinger's equation (-).

β_{ij}, regression coefficients of the statistical models.

γ, coefficient for bead-particle contact (-).

ΔH, enthalpy ($J.g^{-1}$).

ε, volumetric fraction of starch in the suspension (-).

ε_{tot}, total energy dissipation rate ($W.m^{-3}$).

ε_{vis}, energy dissipation rate due to liquid-beads viscous friction and lubrication ($W.m^{-3}$).

ε_{coll}, energy dissipation rate due to partially inelastic bead-bead collisions ($W.m^{-3}$).

ε_{ht}, energy dissipation rate due to shear between liquid layers ($W.m^{-3}$).

η, milling efficiency (-).

η_b, Poisson's ratio of the beads (-).

Θ, granular temperature ($m^2.s^{-2}$).

k, restitution coefficient for bead-bead collisions (-).

k_m, apparent breakage rate constant of the milling process (s^{-1}).

λ, material-dependent factor (-).

μ_L, dynamic viscosity of the milled suspension (Pa.s).

μ_m, viscosity of the stirred media (Pa.s).

ν, stirrer tip speed (s^{-1}).

Π, energy dissipation rate due to the deformation of particles, per unit volume ($W.m^{-3}$).

ρ_b, density of zirconia beads ($kg.m^{-3}$).

ρ_L, density of the milled suspension ($kg.m^{-3}$).

ρ_{bed}, apparent packed density of a bed of grinding media ($kg.m^{-3}$).

ρ_m, density of the stirred media ($kg.m^{-3}$).

σ_b^{max}, maximum contact pressure at the center of the contact circle (Pa).

σ_Y, contact pressure in a material's particle when the fully plastic condition is obtained (Pa).

φ_b, volumetric beads' filling ratio (-).

Ω, empirical coefficient of the Rittinger's equation ($J.m^{\beta-4}$).

1. Introduction.

Starch is a complex polysaccharide extracted from different botanical sources such as corn, potato, wheat or rice, with a great importance in human nutrition (Albert et al., 2019; Sui & Kong, 2018). It is a polymeric carbohydrate consisting of anhydrous glucose units linked primarily through α-D-(1-4) glycosidic bonds. The basic structural units are the linear and helical amylose molecules (20–30%), with an average molecular weight of 106, and the branched amylopectin molecules (70–80%) with a molecular weight of around 1010. Moreover, it naturally occurs as semi-crystalline granules, with a crystallinity index between 15-45% (Patel et al., 2016). Amylose and amylopectin are arranged radially in the starch granule, with their terminal reducing groups oriented towards the center. Hydrogen bonds maintain the integrity of the granules, which contain crystalline and non-crystalline regions in alternating layers (Sui & Kong, 2018). The packing of amylopectin molecules forms dense crystalline areas, which alternate with less dense and amorphous areas due to amylose molecules (Schmiele et al., 2019).

Starch and its derived products exhibit several desirable properties, such as non-toxicity, biocompatibility, biodegradability, availability and low price, which make them an attractive ingredient in food and pharmaceutical formulations (Azad et al., 2021; Rostamabadi et al., 2023). For instance, the main uses of starch derived products in the food industry include the following: adhesive, clouding, film-forming agents, foam stabilizers, bread anti-aging, gelling, glazing agents, emulsion stabilizers, texturizers and thickening agents, among others (Sui & Kong, 2018; Schmiele et al., 2019).

The limitations of native starches for their industrial application are well-known: low solubility at room temperature, retrogradability, opacity of pastes, substantial syneresis of gels, and low resistance against shear/temperature (He et al., 2023; Rostamabadi et al., 2023). To overcome such drawbacks, physical, chemical and enzymatic processes exist. Modification can confer functionalities not found in native starches, leading to notable changes in their technological properties (He et al., 2023). Starch micro and nanoparticles with enhanced redispersion, compared with native starches, are the main focus of the present contribution. They show two main advantages for their use in food and pharmaceutical products. First, the various molecular weights and chemical structures of starch allow diverse modifications, thereby obtaining molecules with different hydrophobicity. Second, structural changes in starch molecules due to heat-induced gelatinization have stabilizing effects (Xu et al., 2020).

These micro and nanoparticles can be produced through precipitation methods or from acid hydrolysis. However, hydrolysis processes involve the use of strong corrosive acids, they require long processing times and have low yields. Furthermore, the manufacture of chemically modified starch particles is complicated and often introduces a variety of hazardous chemicals (Lu et al., 2018). On the other hand, nanomilling in stirred media mills is an efficient process for the preparation of ultrafine materials owing to the ease of operation, construction, high size reduction rate, and low wear contamination (Li et al., 2016; Azad et al., 2021). Therefore, stirred mills have been successfully employed for the formulation of different nanoparticles (Patel et al., 2016).

Size reduction techniques are important during processing of biomaterials, as a first step in biomass conversion (Patel et al., 2016). In particular, wet-stirred media milling (WSMM) is able to comminute materials into smaller sizes than most known dry mills. In addition, recent studies revealed that WSMM has been widely used in the pharmaceutical field because of its robustness, reproducibility and scalability (Azad et al., 2021; Bhakay et al., 2018). The number of stress events per unit time and unit volume, as well as the stress intensity is very high in WSMM. Therefore, the specific energy consumption in stirred mills for producing fine particles is less than that of other mills (Kwade, 2003; Azad et al., 2021). Due to these advantages, WSMM has been previously reported for preparing nanosuspensions of biopolymers, such as cellulose (Dubey et al., 2018; Krishna et al., 2020, 2023), starch (Chen et al., 2010; Patel et al., 2016; Lu et al., 2018; Krishna et al., 2023), and chitosan (Zhang et al., 2012). Moreover, the use of WSMM for the preparation of cross-linked biopolymer nanosuspensions has been recently informed (Azad et al., 2021).

Previously, the pioneering work of Afolabi et al. (2014) presented a modified version of the microhydrodynamic model by Eskin et al. (2005). The milling intensity factor F was introduced as a lumped microhydrodynamic parameter, which captures the effect of process variables on the energy dissipation rate attributed to the deformation of milled particles. In a subsequent contribution, Azad et al. (2021) described the impact of solvents on microhydrodynamic parameters during milling of sodium starch glycolate. Regarding corn starch nanoparticles, Chen et al. (2010), Patel et al. (2016) and Krishna et al. (2023) thoroughly characterized the nanosuspensions obtained with different milling times and starch concentrations. Moreover, Lu et al. (2018) explored the use of corn starch nanoparticles developed via WSMM for the stabilization of Pickering emulsions. However, no mechanistic descriptions of the milling process were provided.

To the best of the authors' knowledge, the main contribution of the present study relies on the use of combined microhydrodynamic, kinetic analysis and optimization tools for the development of physically stable corn starch nanosuspensions. The impact of a correct physical stabilization of particles during milling, previous to any kinetic analysis is addressed. Besides, the applicability of the microhydrodynamic model was assessed in terms of the significant correlations (and their physical meaning) found between the milling intensity factor *F* and the process variables, and between *F* and the kinetic data.

Therefore, the main objectives were the following: 1) To analyze the effect of surfactants (sodium dodecyl sulfate, SDS) and post-milling operations (centrifugation and homogenization) on the physical stability of corn starch nanosuspensions; 2) To study the influence of process variables (starch concentration and bead diameter) on the physical stability of nanosuspensions, the breakage kinetics and microhydrodynamic parameters during milling; 3) To evaluate the impact of the spray drying process of nanosuspensions on the structural changes and redispersion of powders.

2. Materials and methods.

2.1. Materials.

Food-grade corn starch (BUFFALO® 034010, Ingredion™; Ardion SA Complejo Empresarial, Munro, Buenos Aires, Argentina) was purchased from a local distributor (Distribuidora NICCO, Córdoba, Argentina). The chemical composition (AACC, 2000) was the following: moisture (13%), carbohydrates (86.4%), proteins (0.30%), lipids (0.10%), ash (0.20%). The amylose content was 27.51±0.56% (w/w), which was determined according to Gibson et al. (1997) with the Megazyme amylose/amylopectin kit (Megazyme International, Wicklow, Ireland).

Sodium dodecyl sulfate (SDS) (Sigma–Aldrich, Saint Louis, MO, USA) was used as a stabilizer during milling. Other reagents were HPLC or analytical grade.

Zirmil® Yttria zirconia beads (Saint-Gobain ZirPro Köln, Germany) were used for milling experiments, with average sizes of 0.15 mm and 0.50 mm.

2.2. Wet-stirred media milling equipment.

Corn starch nanosuspensions were prepared by WSMM, using a NanoDisp® laboratory scale mill (NanoDisp®, Córdoba, Argentina). This device, as well as the subsequent processing steps are depicted in **Figure 1**. The milling equipment consists of a sealed milling chamber (120 mL), with an external cooling jacket and a coupled motor (Paredes et al., 2020). The motor has a frequency converter, which allows operations up to 60 Hz. The operating temperature was set to 15 °C using cold water circulation with a compact Thermo Haake® cooling circulator (Thermo Fisher Scientific, USA). Other constant process parameters were the beads' filling ratio (0.25 v/v), the stirrer (rotor) tip speed (1600 rpm), which were set according to Paredes et al. (2020), and the milling time (24 h) according to Lu et al. (2018). The other process variables, which were analyzed in a multilevel factorial design (section 2.5) were the starch concentration (c_S) and the bead diameter (d_b).

As shown in Figure 1, starch (1 to 7 % w/v) and SDS (0 to 1 % w/v) were dissolved in Milli-Q water, and their mixtures were gently stirred for 10 min before being placed in the milling chamber. Afterwards, the obtained nanosuspensions were filtered through a 200 ASTM mesh (74 μm) to separate the beads.

The active power under load (P), and the power consumed without suspension or grinding media (P_0) of the mill were measured during milling experiments with a Fluke recorder (model 435-II, N° 37093104 V05.07, Fluke Corporation, Everett, WA, USA) (software Power Log 5.6), with an integration period of 1 min.

2.3. Preliminary experiments: influence of surfactant addition (sodium dodecyl sulfate, SDS) and post-milling operations (centrifugation and homogenization) on the physical stability of nanosuspensions.

According to Wu & Ma (2016), corn starch nanoparticles must show colloidal stability in order to stabilize dispersed systems, such as Pickering emulsions. Moreover, depending on the process conditions (mainly on the bead diameter), a possible bead wear/contamination in some WSMM process has been reported (Li et al., 2016). Therefore, after milling (step 1) and separating the beads (step 2), the obtained suspensions must be centrifuged (step 3) to eliminate any colloidally unstable particle aggregates, as well as any possible contamination from the grinding media (Figure 1). In addition, these nanosuspensions would be used in two forthcoming publications by our group as Pickering emulsions' stabilizers. Given that different homogenization devices are needed to incorporate the oil phase of emulsions, the effect of the homogenization step (step 4 in Figure 1) was analyzed on the physical stability of nanosuspensions.

Owing to the attractive forces between particles and their tendency to aggregation, these biopolymers' suspensions are physically unstable (Li et al., 2016; Xu et al., 2020). The addition of a suitable stabilizer during milling can mitigate the aggregation phenomena, and prevent particle growth due to Ostwald ripening (Li et al., 2016).

Properly stabilized suspensions must be obtained before assessing the influence of milling process variables (section 2.5.1) on the breakage kinetics (section 2.6) and microhydrodynamic parameters (section 2.7). Therefore, sodium dodecyl sulfate (SDS) has been widely used, due to its availability and the electrical repulsion as the main stabilization mechanism (Azad et al., 2021).

Regarding the use of SDS in food applications, it could also be found as Sodium lauryl sulfate, and it is permitted for direct addition to food for human consumption by the Food and Drug Administration (FDA) (Title 21, Volume 3, Part 172; Subpart I: Multipurpose additives; Sec. 172.822: Sodium lauryl sulfate) (CFR - Code of Federal Regulations Title 21 (fda.gov)). According to the FDA regulation, it is used or intended for use as: an emulsifier in or with egg whites, whipping agent, surfactant in dry beverages and fruit juices, and as a wetting agent. The allowed limits for each application are prescribed by the FDA and could be found in the previous link. For instance, it should not exceed 1000 parts per million when used as an emulsifier with egg white. In this regard, it is important to point out that these regulations are specified for the use of pure SDS. However, it is used in combination with other food-grade starch components in the present contribution, yielding complexes that may act as emulsifiers (sections 3.5.2 and 3.5.3). Therefore, the developed nanosuspensions could be used in the required amounts to comply with the FDA regulations for the final concentration of SDS, if they were added as emulsifiers in more complex food matrices.

In view of the above, the effect of different concentrations of SDS (0, 0.01, and 1% w/v) on the physical stability of corn starch nanosuspensions was addressed in this preliminary study. Moreover, the influence of post-milling operations (centrifugation and homogenization) on the physical stability during storage (4 °C±1) of nanosuspensions for one week was studied. For this set of experiments, a corn starch concentration of 1% (w/v), and zirconia beads with an average size of 0.15 mm were used.

As shown in the scheme depicted in Figure 1, after milling and separating the beads, the nanosuspensions were centrifuged (13000 *g* x 40 min). The supernatant was collected and homogenized in two stages: first, with a high speed homogenizer (18000 rpm, 2 min, Ultraturrax IKA T18, Janke & Kunkel GmbH, Staufen, Germany); second, with a high

pressure valve homogenizer (2 cycles at 500 bar, EmulsiFlex C5, Avestin, Ottawa, ON, Canada).

Each milling condition of the preliminary experiment was evaluated in triplicate. Then, the obtained nanosuspensions after each step were characterized as described in section 2.4. Finally, the SDS concentration that yielded the most stable nanosuspensions was subsequently used in optimization and breakage kinetic experiments.

2.4. Characterization of nanosuspensions:

The nanosuspensions after each step described in section 2.3 were characterized in triplicate as follows:

2.4.1. Particle size distribution and zeta potential.

The average particle size (Z_{av}) and the polydispersity index (PDI) of nanosuspensions immediately after milling and post-processing, and after storage for one week, were determined by dynamic light scattering (Nano Zetasizer, Malvern Instruments, Worcestershire, UK). The zeta potential was also determined with the same equipment. The measurements were carried out at 25 °C and the equilibration time was 120 s (Bordón et al., 2021a).

2.4.2. Rheological behavior.

The rheological behavior of the parent starch suspensions and of the obtained nanosuspensions was assessed with a controlled-stress rheometer, Physica MCR 301 Anton Paar (Physica Messtechnik, Ostfildern, Germany). A plate-cone geometry (1°, 50 mm diameter) was used, working with a 0.05 mm-gap, and the measurements were carried out at 25 °C (Bordón et al., 2021a).

2.5. Wet-stirred media milling experimental design.

Wet milling is a time consuming operation, and the energy efficiency is usually low (Afolabi et al., 2014; Eskin et al., 2005). Therefore, it is crucial to achieve the operation efficiency through process optimization techniques. In order to enhance the milling process, the relationship between experimental factors and dependent variables must be predictable. With that aim, the Response Surface Methodology (RSM) was applied with the aid of statistical software (STATGRAPHICS®, Statpoint Technologies, Warrenton, VA, United States).

A multilevel factorial experimental design was carried out with the NanoDisp® mill. The effects of starch concentration c_S (1, 3.5 and 7% w/v), the bead diameter d_b (average sizes of 0.15 and 0.50 mm), and their interaction, were analyzed on eight response variables. Six different combinations of c_S x d_b (1 x 0.15; 1 x 0.50; 3.5 x 0.1; 3.5 x 0.50; 7 x 0.1; 7 x 0.50) were explored and the experiments were carried out in triplicate. The analyzed response variables were: initial and final average particle size ($Z_{av,0}$, $Z_{av,f}$, $Z_{av,0,c}$, $Z_{av,f,c}$) and polydispersity index (PDI_0, PDI_f, $PDI_{0,c}$, $PDI_{f,c}$). The subscripts "0", "f" and "c" indicate "initial" and "final" (after storage for one week) values, and "centrifugation" of samples, respectively. Hence, the particle size parameters of nanosuspensions were analyzed before and after centrifugation.

2.5.1. Optimization.

The first step for process optimization with RSM is to transform each response surface function (Y_i') into the corresponding individual desirability function (d_i). Then, all the individual desirability functions are combined into the global desirability function (D_G) as the only optimization objective (Statpoint Technologies, 2010). The statistical software provides a quadratic polynomial expression as a regression model for each response:

$$Y' = \beta_0 + \beta_1 X_1 + \beta_2 X_2 + \beta_{12} X_1 X_2 + \beta_{11} X_1^2 \qquad \text{(Eq. 1)}$$

where Y' is the modeled response, β_0, β_i, β_{ii} and β_{ij} are the constant term, the linear, quadratic and interaction coefficients, respectively; X_1 and X_2 are the starch concentration and the bead diameter, respectively.

The accuracy of the regression models was assessed with the determination coefficient (R^2), the absolute average deviation (AAD), the bias (B_f) and accuracy factors (A_f) calculated according to Bordón et al. (2021b).

Once the regression models were fitted, they were combined in the unique desirability function to determine the optimum process condition (c_S x d_b) that simultaneously optimized the response variables within the experimental domain (Bordón et al., 2021b).

$$D_G = \left(\prod_i^m d_i^{I_i}\right)^{\left(\frac{1}{\sum I_i}\right)} \qquad \text{(Eq. 2)}$$

where m is the number of responses. The global desirability function D_G varies from 0 (completely undesirable) to 1 (fully desirable).

Impact coefficients (I_i) were incorporated to take into account the importance of one response over the others. Usually, the impact coefficients vary from 1 to 5 (Statpoint Technologies, 2010). STATGRAPHICS® sets 1 as the default impact coefficient for all the optimized variables. In this contribution, all the impact coefficients were left at this default value, except for $Z_{av,0,c}$ and $Z_{f,c}$, for which I=3. This decision was made based on two aspects. First, the colloidal stability of nanoparticles is of utmost importance. Second, different international standards established PDI<0.05 and PDI>0.7 as typical of monodisperse and polydisperse samples, respectively (ISO 22, 412:2017). However, this index is difficult to control in complex samples such as food ingredients (Amparo et al., 2018).

2.6. Corn starch breakage kinetics.

A sound understanding of the breakage kinetics allows determining the milling time and the production rate for a target particle size (Afolabi et al., 2014). In order to adjust the breakage kinetic models described in this section, the particle size data of the experimental runs in the multilevel factorial design (section 2.5) was used. To avoid large errors due to particle aggregates or contamination from the grinding media, the kinetic models were adjusted to the particle size data measured after centrifugation (step 3 of Figure 1).

The size reduction rate (*SRR)* can be defined as a first-order kinetic model, where $-dd_{50}/dt$ (Eq. 3) represents the change in the median of the size distribution, d_{50} (nm) as a function of the milling time (s). SRR depends on the particle size, process conditions (microhydrodynamics) and material's properties (Azad et al., 2021).

$$SRR = \frac{-dd_{50}}{dt} = k_m(d_{50} - d_l) \quad \text{(Eq. 3)}$$

The integration of the above equation yields the following expression:

$$d_{50}(t) = d_l + [d_{50}(0) - d_l]e^{-k_m t} \quad \text{(Eq. 4)}$$

When the breakage of particles governs the milling process and surpasses the aggregation phenomena, d_{50} decreases monotonically from the initial $d_{50}(0)$ to a limiting value (d_{lim}) (Afolabi et al., 2014; Azad et al., 2021). Experimental data obtained for different materials suggest that the evolution of the average particle size follows a first-order exponential decay, which is described by the apparent breakage rate constant k_m (s^{-1}) (Afolabi et al., 2014).

Previously, Azad et al. (2021) applied Eq. 5 for the WSMM of sodium starch glycolate. During the first 30 min, d_{50} decreased monotonically. Since in our contribution d_{lim} was not reached during the first 30 min of milling, and the median diameter values recorded were

above d_{lim} in the absence of aggregation (d_{50}>>d_{lim}), the following form of the above model in Eq. 4 was adjusted to the kinetic data:

$$d_{50}(t) = d_{50}(0)e^{-k_m t} \quad \text{(Eq. 5)}$$

2.7. Microhydrodynamic analysis.

The physical model proposed by Eskin et al. (2005), which was subsequently modified by Afolabi et al. (2014), was applied in this study. This approach is known as "Microhydrodynamic model", and describes the effects of milling process variables on the breakage kinetics and on the dynamics of the grinding media (microhydrodynamic parameters) at the microscopic level (Afolabi et al., 2014). The model was applied as a practical approach to estimate the energy consumed for the deformation of solids, which can be used as a general criterion for the milling efficiency.

In the present contribution, only the salient features and main equations are presented. The main assumptions and derivations are well described by Eskin et al. (2005) and Afolabi et al. (2014). The equations were implemented and solved in MATLAB software (R2019a), and the granular temperature (Eq. 11, section 2.7.2) was calculated with the inbuilt *fsolve* function.

2.7.1. Applicability of the model

Under turbulent flow conditions (Re>35000), the energy consumed in liquid mixing is transformed into kinetic energy of turbulent fluctuations, because the turbulent viscosity is much greater than the laminar viscosity (Eskin et al., 2005). Therefore, the Reynolds number must be calculated to assess the applicability of the model:

$$\Re = \frac{vD^2\rho_m}{\mu_m} \quad \text{(Eq. 6)}$$

where v (s^{-1}) is the tip speed (26.67 s^{-1}), D (m) is the rotor diameter (0.06 m), ρ_m ($kg.m^{-3}$) and μ_m (Pa.s) are the density and viscosity of the stirred media, respectively. In turn, ρ_m and μ_m (in the presence of beads) are calculated as follows:

$$\rho_m = \rho_b c + \rho_L(1-c) \quad \text{(Eq. 7)}$$

$$\mu_m = \mu_L(1 + 2.5c + 10c^2 + 0.0019e^{20c}) \quad \text{(Eq. 8)}$$

where ρ_b is the density of zirconia beads (6000 $kg.m^{-3}$), ρ_L ($kg.m^{-3}$) and μ_L (Pa.s) are the density and viscosity of the equivalent liquid (milled suspension), respectively, and c (-) is the bead volume fraction in the milling chamber.

In Eq. 7, the density of the milled suspensions was determined with a 25 mL-pycnometer according to Bordón et al. (2021b). Moreover, in Eq. 8, the viscosity of suspensions was measured as described in section 2.4.2 (rheological behavior).

In turn, the bead volume fraction *c* was calculated with Eq. 9:

$$c = \varphi_b \left[1 - \left(1 - \frac{\rho_{bed}}{\rho_b}\right)\right] = \varphi_b \frac{\rho_{bed}}{\rho_b} \quad \text{(Eq. 9)}$$

where φ_b is the filling ratio of the beads (0.25 v/v), ρ_{bead} and ρ_b are the apparent packed density of the bed and the true density of the grinding media, respectively.

2.7.2. Granular temperature

In a stirred mill, the power applied by the mill stirrer per unit volume, P_w (W.m^{-3}) is dissipated through fluctuations on the microscale, and is equal to the total energy dissipation rate, ε_{tot} (W.m^{-3}) according to Eq. 10. In turn, P_w is deduced from P-P_0, where P (W.m^{-3}) and P_0 (W.m^{-3}) are the power applied by the mill motor and the power consumed with no load per unit volume, respectively. Both P and P_0 were measured with the Fluke recorder (section 2.2).

$$\varepsilon_{tot} = P_w = \varepsilon_{vis} + \varepsilon_{coll} + \varepsilon_{ht} \quad \text{(Eq. 10)}$$

where ε_{vis}, ε_{coll} and ε_{ht} (W.m^{-3}) are the energy dissipation rates due to viscous friction between the liquid and the grinding media, due to inelastic collisions between grinding media, and due to shear between liquid layers of suspensions, respectively. In the above equation, ε_{ht} was added by Afolabi et al. (2014) for the energy dissipation in transition regimes (120<Re<35000).

The deduction of each dissipation term in Eq. 11 are explained by Eskin et al. (2005) and Afolabi et al. (2014):

$$P_w = \frac{54\mu_L c\theta R_{diss}}{d_b^2} + \frac{12}{d_b\sqrt{\pi}}(1-k^2)\frac{1-0.5c}{(1-c)^3}\varrho_b\theta^{3/2}P_{ht}\varepsilon \quad \text{(Eq. 11)}$$

In the above equation, θ (m^2.s^{-2}) is the granular temperature, which is a fundamental microhydrodynamic parameter defined as the bead-liquid relative mean square velocity. It was solved from Eq. 11 with the *fsolve* inbuilt function, and the rest of the parameters were estimated from θ.

The first term in the right side of Eq. 11 is equal to ε_{vis}, and R_{diss} (-) is the effective drag coefficient of the grinding media (Afolabi et al., 2014). The second term is equal to ε_{coll}, being *k* the restitution coefficient for the bead-bead collisions taken as 0.76 according to

Afolabi et al. (2014) and Tatsumi et al. (2009). Finally, the third term in the right side of Eq. 11, $P_{ht}\varepsilon$ is equal to ε_{ht}, where P_{ht} (W.m^{-3}) is the power consumed per unit volume when stirring the suspension in the absence of grinding media, and ε (-) is the volume fraction of corn starch in the suspension.

For the sake of brevity, the equations to calculate R_{diss} as a function of the bead concentration c are not presented here. The reader may consult the Appendix A of the publications by Afolabi et al. (2014) and Azad et al. (2021), in which the equations are given in detail.

2.7.3. Milling intensity factor, *F*

For many kind of mills, the equation relating the specific energy spent on grinding and the average particle size Z (m) is the following (Eskin et al., 2005):

$$dE = -\Omega \frac{dZ}{Z^{\beta}} \qquad \text{(Eq. 12)}$$

where β (-) and Ω (J.m$^{\beta-4}$) are empirical coefficients, and dE (J.m^{-3}) is the elementary specific energy spent on grinding.

By integrating Eq. 12 into separate variables, and considering β=2 (Eskin et al., 2005), the Rittinger's law for fine grinding is obtained:

$$E = \Omega \left(\frac{1}{Z} - \frac{1}{Z_0}\right) \quad \text{(Eq. 13)}$$

Through the analysis of tensions exerted on a particle trapped between two beads and the probability of this entrapment, the energy dissipation rate dE/dt can be derived (Eq. 14). For the sake of brevity, the whole deduction is not presented here. The reader may consult the work of Eskin et al. (2005) for more details.

$$\Pi = \frac{dE}{dt} = \lambda F \quad \text{(Eq. 14)}$$

In Eq. 14, dE/dt or Π (J.m^{-3}.s^{-1}) is the energy dissipation rate resulting from particles' deformation per unit volume. This magnitude characterizes the grinding intensity and can be used as an efficiency criterion (Afolabi et al., 2014). The energy dissipation rate contains two factors: λ (kg.m$^{-3.6}$.s$^{-0.4}$) or material-dependent factor, and F (m$^{2.6}$.s$^{-2.6}$), the milling intensity factor dependent on the process conditions:

$$\lambda = \frac{1}{\pi^{5/2}\sigma_Y}\left(\frac{Y_b}{1-\eta_b^2}\right)^{18/15}\left(\frac{Y}{Y_p}\right)^{\gamma}\varrho_b^{4/5}\frac{\left(\frac{Z}{2}\right)}{\frac{d_b}{2^2}} \quad \text{(Eq. 15)}$$

$$F = \frac{c^2(2-c)}{(1-c)^3}\frac{1}{\varepsilon}\theta^{13/10} \qquad \text{(Eq. 16)}$$

In Eq. 15, λ encompasses mechanical properties of the milled material (the Young modulus Y_b, the contact pressure in a material's particle when the fully plastic condition is obtained or σ_Y, and the reduced elastic modulus for the bead-particle contact Y^*) and of the beads (the Young modulus Y_b and the Poisson's ratio η_b). However, the material's mechanical properties are usually not available in the open literature, or their experimental determination is difficult to perform (Azad et al., 2021; Parker et al., 2020). The material-dependent factor λ is essentially constant for specific sizes. Therefore, the changes in the operation variables are reflected in the milling intensity factor F according to Eq. 16. An increase in F is automatically associated with a faster formation of finer particles (Afolabi et al., 2014). In this regard, the main practical implication of this approach relies on the direct impact of the changes in F on Π, regardless of the material's mechanical properties (Azad et al., 2021).

2.7.4. Average frequency of corn starch particle compressions, *a*

The average frequency of particle compressions and the maximum contact pressure are useful for a qualitative description of grinding phenomena at the microscopic level (Afolabi et al., 2014). Both were calculated according to Afolabi et al. (2014) and Azad et al. (2021):

$$a = 5.82 \frac{1}{\sqrt{\pi}} \frac{c^2(2-c)}{(1-c)^4} \left[\varrho_b \frac{(1-\eta_b^2)}{Y_b} \right]^{2/5} \theta^{9/10} \frac{R_p}{\left(\frac{d_b}{2}\right)^2} \quad \text{(Eq. 17)}$$

where R_p is the particle radius (m). For zirconia beads, Y_b (265 GPa) and η_b (0.27) can be obtained from Flach et al. (2018).

2.7.5. Maximum bead contact pressure at the center of the bead contact circle, σ_b^{max}

The maximum contact pressure was calculated with the following equations according to Afolabi et al. (2014):

$$\sigma_b^{max} = \frac{3}{2} \frac{F_b^n}{\pi \alpha_b^2} \quad \text{(Eq. 18)}$$

where F^n_b (N) is the maximum average normal force during collision of two elastic beads, and α_b (m) is the radius of the contact circle at the contact point of two beads. Moreover, these two terms were calculated as follows:

$$F_b^n = 1.96 \left(\frac{Y_b}{1-\eta_b^2} \right)^{2/5} \rho_b^{3/5} \left(\frac{d_b}{2} \right)^2 \theta^{3/5} \quad \text{(Eq. 19)}$$

$$\alpha_b = \left[\frac{3}{4}\frac{(1-\eta_b^2)}{Y_b}\left(\frac{d_b}{2}\right)F_b^n\right]^{1/3} \quad \text{(Eq. 20)}$$

Finally, Y_b, η_b, ρ_b and d_b are properties of the beads, as described above in sections 2.7.1 and 2.7.3, and θ is the granular temperature introduced in section 2.7.2.

2.8. Spray drying of corn starch nanosuspensions.

In order to obtain redispersible powders, and with the highest total solid concentration within the experimental domain (section 2.5), specific corn starch nanosuspensions (c_S of 7% w/v and SDS concentrations of 0, 0.7 and 1% w/v) were spray dried. For the preparation of these nanosuspensions, zirconia beads with an average d_b of 0.15 mm were used. The three feed formulations were spray dried in triplicate, in a laboratory scale spray dryer (Mini Spray Dryer Büchi B-290, Büchi Labortechnik, AG, Switzerland) equipped with a twin-fluid nozzle atomizer (0.7 mm). The combination of spray drying process variables was based on Fu et al. (2012), with brief modifications: drying-air inlet temperature (117±1 °C), outlet temperature (65±1 °C), atomization flow rate (1054 $L.h^{-1}$), feed flow rate (2.8 $mL.min^{-1}$), drying-air flow rate (38 $m^3.h^{-1}$).

Afterwards, the powders obtained were characterized in triplicate as follows:

2.8.1. Particle size.

The particle size distribution of the resuspended powders was determined by dynamic light scattering according to section 2.4.1, with modifications. Previously, the necessary amount of powder was weighed and then resuspended in Milli-Q water, in order to yield a final solid concentration of 1% (w/v). This concentration was selected to avoid multiple scattering effects (Bordón et al., 2021a).

2.8.2. Differential scanning calorimetry.

The thermal analysis of starch samples and SDS was performed with a differential scanning calorimeter (DSC 823e, Mettler Toledo, Greifensee, Switzerland) according to Piloni et al. (2022), with modifications. Starch samples (8 mg) were weighed and placed in 40 μL

aluminum pans. Then, distilled water was added with a Hamilton microsyringe to yield a 1:3 (w:w) solid:water ratio. For SDS samples, 10 mg of dry powder were weighed in the aluminum pans. These pans were hermetically sealed, and allowed to stand for 24 h at room temperature before analysis. Starch and SDS samples were subjected to the following conditions: 25 °C for 5 min, and then heating up to 120 °C at 10 °C/min. For all measurements, an empty and sealed pan was used as reference. Finally, the enthalpy of different endothermic events (ΔH), the onset, peak and endset temperatures (T_0, T_p and T_e, respectively) were informed.

2.8.3. X-ray diffraction.

X-ray diffraction (XRD) patterns of starch samples and SDS were obtained with a diffractometer Philips PW1800 (USA), as described by Piloni et al. (2022). The patterns were obtained with Cu kα radiation (λ = 0.154 nm), with the following operating conditions: 30 mA, 40 kV, 2–40° scanning region (2θ), and a scanning speed of 0.01°/s. Spectrum fitting and crystallinity percentage were calculated using OriginPro software (version 8.5, OriginLab®, Northampton, Massachusetts, USA).

2.8.4. Transmission electron microscopy (TEM).

The morphology and size of particles after spray drying and resuspension were assessed by transmission electron microscopy, using a Hitachi HT7800 microscope (Hitachi High-Tech Corporation, Japan) with a resolution of 0.20 nm and an acceleration voltage of 20-120 kV. Prior to the analysis, powder samples were resuspended in Milli-Q water to achieve a final concentration of 2.5% (w/v), and a drop of the suspension was deposited on grids covered by a plastic membrane to prevent the liquid sample from slipping.

2.9. Statistical analysis.

All the mean values reported for the analytical determinations are the average of triplicate measurements. Multivariate analysis of variance (ANOVA) was applied at 5% level of significance, using the STATGRAPHICS® statistical program. The influence of the formulation and process variables and their interaction on dependent variables was analyzed. In those cases where statistically significant differences ($p<0.05$) were observed, a multiple comparison of means by the Fisher's test was applied.

3. Results and discussion.

3.1. Preliminary experiments: influence of surfactant addition (sodium

dodecyl sulfate, SDS) and post-milling operations (centrifugation and homogenization) on the physical stability of nanosuspensions.

Table 1 shows the particle size distribution parameters and zeta potential of nanosuspensions, which were obtained via WSMM of starch suspensions with an initial average particle size of 14.08±0.08 μm. The particle sizes of fresh nanosuspensions, and after their storage for one week, are given. For these preliminary experiments, a starch concentration of 1% (w/v) and three concentrations of SDS (0, 0.01 and 1% w/v) were explored, as can be seen in Table 1. In this regard, it is important to highlight the pH values of the systems during the particle size and zeta potential measurements, which were between 6.50 – 6.83. Moreover, no noticeable pH changes were observed during storage of nanosuspensions.

Multifactorial ANOVA indicated a significant influence ($p<0.05$) of the SDS concentration, of the processing to which each sample is subjected after milling (centrifugation "C", homogenization "H", and centrifugation followed by homogenization "C+H"), and of the interaction between both factors on particle size parameters. In this regard, **Fig. 2a** shows the evolution of the average particle size of nanosuspensions during the storage for one week. Samples obtained after milling only (1% (w/v) S, 1% (w/v) S+ 0.01% (w/v) SDS, and 1% (w/v) S+ 1% (w/v) SDS), or followed by centrifugation and homogenization steps (1% (w/v) S+C+H, 1% (w/v) S+ 0.01% (w/v) SDS+C+H, and 1% (w/v) S+ 1% (w/v) SDS+C+H) are shown. Moreover, **Figures 2 b** to **d** depict the initial particle size distributions of all samples, also including those obtained after milling and centrifugation only (1% (w/v) S+C, 1% (w/v) S+ 0.01% (w/v) SDS+C, and 1% (w/v) S+ 1% (w/v) SDS+C), or milling followed by homogenization (1% (w/v) S+H, 1% (w/v) S+ 0.01% (w/v) SDS+H, and 1% (w/v) S+ 1% (w/v) SDS+H).

Fig. 2a suggests the mandatory need to apply post-milling operations to milled starch particles. Indeed, there is a notable increase in the particle size of starch samples without the addition of SDS, and with no post-milling operations. This latter is clear evidence of destabilization phenomena in corn starch nanosuspensions.

The homogenization step is applied after centrifugation because Pickering emulsions will be prepared and studied in two forthcoming publications by our group. For the same SDS concentration (see Table 1), and for the studied starch concentration in this preliminary study (1% w/v), no statistically significant difference ($p>0.05$) was found between the average particle size of only centrifuged ("C"), and centrifuged and homogenized samples ("C+H"). This suggests the necessity to apply a greater energy during the homogenization step to achieve the breakdown of such small particles. There is a limit particle size achievable during homogenization, despite the application of a large amount of energy. Moreover, only a small

fraction of the applied energy is used to create new surface area, and the rest is dissipated as heat (Schultz et al., 2004). On the other hand, sedimented particles were observed after one week in those nanosuspensions that were homogenized only, without going through a previous centrifugation step (Figure 1).

In order to achieve a proper electrostatic charge of the dispersed corn starch nanoparticles, SDS was added as a stabilizer during milling. The addition of SDS allows for adequate wetting of particles during milling and prevents their aggregation, besides conferring a net electrostatic repulsion (Li et al., 2016). According to Table 1, the nanosuspensions formulated with 1% (w/v) of SDS exhibited significantly higher ($p<0.05$) values of $Z_{av,0}$, $Z_{av,f}$, PDI_0 and PDI_f, compared with 0 and 0.01% (w/v) of SDS. The highest proportion of surfactant evaluated in this study exceeded the critical micellar concentration (CMC) at 25 °C (0.23% w/v in the absence of any other additive) (Zhang et al., 2019). Above this CMC, surfactant micelles are spontaneously formed, which could induce deviations during particle size and zeta potential measurements. On the other hand, a concentration of 0.01% (w/v) yielded an enhanced physical stability over time (Figure 2a and Table 1), especially after the centrifugation step. These observations demonstrate that the use of a proper amount of SDS is crucial for the physical stability of nanosuspensions.

Like in the present contribution when no stabilizer was added, Patel et al. (2016) also observed an increase in the particle size of corn starch nanosuspensions during storage. Recrystallization of amylose molecules occurs quickly after cooling of gelatinized starch samples. On the other hand, the recrystallization of amylopectin molecules is a slower process, which involves the reassociation of their external branches (Schmiele et al., 2019). In our study, gelatinization of starch occurred during milling (see section 3.5.2), and the samples were immediately stored at 4 °C for one week.

Regarding the interaction between starch and SDS, it has been argued that amylose molecules in aqueous solution form left-handed helices with an internal hydrophobic cavity, where ligands can reside (Hay et al., 2019). These ligands can produce non-retrograding complexes with amylose, which remain soluble due to the electrostatic repulsion of their ionic groups (Putseys et al., 2010). Therefore, the formation of non-retrograding complexes between the amylose molecules leached during milling and the SDS added may occur in the present contribution. This would support the use of SDS as a stabilizer during milling in our study, since the formation of amylose complexes drastically alters the properties of starch, allowing its use in many relevant applications (Hay et al., 2019). These complexes exhibit enhanced solubility and emulsifying capacity, compared with amylose and the ligand molecules on

their own (Hay et al., 2019; Putseys et al., 2010). Additional evidence of the formation of these non-retrogradading complexes is discussed in section 3.5.2.

3.2. Optimization of the wet-stirred media milling process.

After defining a suitable proportion of SDS for the correct physical stabilization of nanosuspensions in section 3.1 (1% w/w of the total starch concentration present in the formulation), a multilevel factorial experimental design for the WSMM process was carried out. For each milling condition, the solid content of nanosuspensions were determined after centrifugation, with a moisture analyzer operated with infrared heating according to Bordón et al. (2021a). The values are given in **Table S1** of the Supplementary Material. Moreover, the solid yield (%, dry basis) was calculated considering the initial amount of solids added into the formulation. As explained above in section 3.1, the centrifugation step after milling and separating the beads was applied in order to eliminate colloidally unstable particle aggregates, and any possible contamination from the grinding media. Given the total solid content of the supernatants, the solid yield values (>80%) in Table S1 indicate a high amount of solids recovered after milling and centrifugation. In addition, these results highlight an acceptable colloidal stability of nanosuspensions, in contrast to the easily – sedimentable particles of native starch suspensions.

The influence of starch concentration (c_S), the bead diameter (d_b), and their interactions on particle size parameters and zeta potential of nanosuspensions was assessed. **Table S2** in the Supplementary Material shows the significant effects of the experimental factors on the response variables, the regression coefficients of the adjusted statistical models, their level of significance, and the goodness-of-fit of the models. Good fits were obtained for average particle sizes ($Z_{av,0}$, $Z_{av,f}$, $Z_{av,0,c}$, $Z_{av,f,c}$), for which statistically significant influences ($p<0.05$) of all experimental factors, interaction and quadratic effects were observed. In addition, the percentage absolute average deviation (AAD) was below 5% for the particle size regression models, highlighting a good fit. Regarding the PDI, no significant influences ($p>0.05$) of the experimental factors were evident, except after centrifugation. Poor fits of the regression models were also observed, which might be attributed to the behavior of the PDI in complex samples such as food suspensions (Amparo et al., 2018).

Table 2 gives the observed values of the response variables, for all the experimental conditions. In this regard, it is worth pointing out the initial particle size values observed before centrifugation ($Z_{av,0}$) for the same process conditions (c_s = 1% w/v, 0.01% w/v SDS and a d_b= 0.15 mm). There were significant differences between the values recorded in the preliminary study of section 3.1 ($Z_{av,0}$=444 nm, Table 1) and in the multilevel experimental

design ($Z_{av,0}$=220 nm, Table 2). This latter observation evidences the wide variety of chain lengths and sizes of starch compounds obtained via WSMM (Chen et al., 2010), due to the complex nature and molecular organization of the granules. Therefore, the complex molecular organization of the milled material might account in part for the differences between the values of Table 1 and 2. On the other hand, the difference was dramatically reduced after centrifugation, for the same process condition: $Z_{av,0,c}$ values of 182 nm and 152.55 nm in Table 1 and 2, respectively. In view of the enhanced reproducibility of the experimental results after centrifugation, these latter were further used to adjust the breakage kinetic models (section 3.3) and for the microhydrodynamic analysis (section 3.4).

As can be seen from Table 2, as c_S increases for a constant d_b, particle breakage becomes difficult. Afolabi et al. (2014) concluded that by increasing the concentration of the solid in suspensions, a smaller fraction of nanoparticles is obtained and the breakage kinetics are slower. Moreover, using smaller zirconia beads leads to a lower maximum contact pressure between them, but to a dramatic increase in the frequency of particles' compressions. The overall impact of the bead diameter d_b will depend on which of these two opposing effects are more pronounced, and how they relate to the mechanical properties of the specific solid (Li et al., 2016). In our study, the effect of the increase in the contact pressure when using beads with a larger d_b seems to exceed the decrease in the frequency of particles' compressions. Therefore, the milling operation is more efficient with a larger d_b (Li et al., 2016; Azad et al., 2021).

In order to find the optimal combination of c_S x d_b that yields the optimization goals described in section 2.5.1, the statistical software combined the individual desirability of each regression model generated for the independent variables. Within the explored domain, the optimal combination of experimental factors yielded a global desirability value of 0.856, as shown in the response surface plot of **Figure 3**. As can be seen, the optimal c_S and d_b were 2.48% (w/v) and 0.50 mm, respectively. This optimal combination of process variables was experimentally validated in triplicate, and under these conditions, $Z_{av,0}$ and $Z_{av,0,c}$ values were 313.87± 1 and 153.90±3 nm, respectively. The rest of the responses observed with the optimal process conditions are given in **Table 3**. Moreover, a prediction error was calculated between observed and predicted responses under these conditions. The predictions for the most relevant variables ($Z_{av,0}$, $Z_{av,f}$, $Z_{av,0,c}$, $Z_{av,f,c}$) were acceptable, since errors below 12% were observed. On the contrary, the largest deviations were observed for the PDI, in accordance with the poor fits of the regression models. According to Table 3, $Z_{av,0} > Z_{av,f}$ in non-centrifuged samples. This might be attributed to the sedimentation of particles without

colloidal stability during storage, which was also reported by Patel et al. (2016) in corn starch nanosuspensions.

The rheological behavior of parent starch suspensions and of the obtained nanosuspensions was studied, as an important input for the microhydrodynamic model (section 3.4). **Table S3** of the Supplementary Material summarizes the calculated Power law parameters: the consistency index (K_i) and the flow index (n). Moreover, **Figures 4a** to **c** show the shear stress as a function of the shear rate. All values of the flow index n were close to 1. Therefore, all the samples exhibited a Newtonian behavior, and their consistency index K_i is equivalent to their dynamic viscosity. The suspensions containing a c_S of 7% (w/v) were significantly ($p<0.05$) more viscous than the rest, which is due to the higher solid concentration in the formulation.

As can be seen in Figures 4a to c, the nanosuspensions are more viscous than the parent starch suspensions. In addition, zirconia beads with a larger d_b yielded more viscous nanosuspensions. This might be attributed to an enhanced swelling of particles due to a greater structural damage to starch granules, which increases the leaching of amylose (Ahmad et al., 2020). Moreover, the enhanced swelling of wheat and corn starch granules (and the earlier onset of the gelatinization event) in the presence of different proportions of SDS has been reported previously (Svensson et al., 1998). These observations are consistent with multifactorial ANOVA, which showed significant ($p<0.05$) influences of c_S, d_b and c_S x d_b on K, and the sole significant effect of d_b on n.

Finally, it is worth pointing out the stability of particle size in nanosuspensions after centrifugation during storage for one week ($Z_{av,0,c}$ and $Z_{av,f,c}$, columns 6 and 7, Table 2). Despite the absolute values of ζ-potential recorded below 30 mV with the addition of SDS (1% w/w of the starch concentration), the storage stability observed might be attributed to a combination of electrical and steric mechanisms. This latter may be explained by the increase in viscosity due to amylose leaching (Ahmad et al., 2020) during milling, compared with the parent starch suspensions, especially at starch concentrations of 3.5 and 7% (w/v) (Table S3, Fig. 4b and c).

3.3. Corn starch breakage kinetics.

Figures 5a to **c** show the experimental breakage kinetics for different process conditions, and the adjusted exponential models. According to various authors (Afolabi et al., 2014; Azad et al., 2021; Parker et al., 2020), an exponential decay of particle size is achieved when the breakage rate during milling exceeds that of other mechanisms, such as particle growth or

aggregation. For this reason, a correct stabilization of the parent suspensions is essential (Afolabi et al., 2014; Parker et al., 2020). If the parent suspensions are properly stabilized, the median diameter or d_{50} falls monotonically with time, and a limiting value (d_{lim}) is reached if the milling operation is prolonged.

Equation 5 was adjusted to the experimental data. The breakage kinetic constant k_m and the goodness of fit, R^2 are given in **Table 4**. Various conditions of the experimental design exhibited a good fit, with R^2 values greater than 0.9, except for those experiments carried out with an average d_b of 0.15 mm and c_S values of 3.5 and 7% (w/v). In these latter experiments, Eq. 5 does not accurately represent the comminution phenomena (Azad et al., 2021).

The k_m values obtained show the rate of each milling process. The effects of all the independent variables were statistically significant ($p<0.05$). In general, the faster breakage was observed for lower c_S, and higher d_b values. Increasing the number of particles in suspension causes a decrease in the compression force applied to each individual particle. Hence, the breakage rate is reduced. On the other hand, the intensity of collisions predominates over their frequency when working with larger zirconia beads (Afolabi et al., 2014). These results will be discussed in more detail in the next section.

As can be seen in Table 4 and Figures 5a to c, not all the milling conditions yielded a rapid decay of the particle size towards a plateau value during the early stages of the operation. Indeed, the particle size does not fall monotonically, except for the conditions with the largest d_b (R^2 greater than 0.9). Previously, Azad et al. (2021) studied the nanometrization of sodium starch glycolate in stirred mills. In this situation, the carboxymethylation of starches accelerates the swelling of the granules, whcih facilitates a rapid breakdown of these materials below 1 μm.

In the present contribution, the milling chamber was refrigerated with circulating water at 15 °C. Moreover, it has been previously reported that the water retention capacity of native corn starch granules increases during milling (Chen et al., 2010). Therefore, it is difficult to achieve a rapid swelling at the temperature of circulating water (15 °C) during milling. However, swelling may be enhanced with those process conditions that generate a greater damage to the material (for instance, with a larger bead diameter). In addition, to allow rupture phenomena to govern particle aggregation, correct and rapid stabilization by SDS must be achieved. For a ligand such as SDS to form colloidally stable complexes with soluble starch material, gelatinization of the granules must have begun (Putseys et al., 2010). Once again, this involves rapid swelling of the granules, which is known to be favored by the presence of emulsifiers like SDS in food applications (Biliaderis, 2009).

Finally, the above phenomena support the use of SDS in our contribution, to enhance the swelling of the granules and to achieve a faster breakage kinetic.

3.4. Microhydrodynamic analysis.

The power required to mix non-aerated fluids depends on the stirrer tip speed, impeller size and shape, the tank geometry, and the density and viscosity of fluids (Doran, 1995). It is difficult to calculate the power consumed in a stirred mill due to the wide variety of impellers available. The microhydrodynamic analysis indicates that the milling efficiency is strongly related to the energy dissipation rate. It could be assumed that, if different impellers generate the same energy dissipation rate, then the same milling efficiency would be observed. However, the distribution of the energy dissipation rate may not be uniform within the chamber, and this heavily depends on the impeller type (Eskin et al., 2005). Due to this reason, the power consumed during each experiment was recorded and processed. For all the experimental runs, the active power at the beginning of the operation was 45 W, and a final value of 41 W was observed. In addition, the average power consumed with no load was 40 W. This implies that the power actually consumed by the process varied from 5 to 1 W. For further calculations, an average power consumption of 3 W was taken, as an average of the initial and final values recorded.

The NanoDisp stirred mill used in this work has a squirrel cage motor, which operates by induction. Its rotor is made up of a set of conducting bars parallel to the axial direction, which are arranged in a cylindrical shape around the axis. This motor type is preferred for industrial uses (Zapata, 2021). It is oversized for this application, since it delivers much greater power (0.5 HP or 372.85 W, according to the manufacturer) to that necessary for the creation of new surface area. Therefore, no significant differences were found in the measurement of active power for different milling conditions. As a consequence, the possible fluctuations of P_w due to changes in cs and d_b within the experimental domain are negligible compared to the nominal power supplied by the motor.

Table S4 of the Supplementary Material shows all the calculated microhydrodynamic parameters for different milling process conditions. In the development of the microhydrodynamic model, the third term of Eq. 10 accounts for the energy dissipation due to friction between liquid layers (ε_{ht}), if the flow regime falls within the zone transition ($120<Re<35000$) in the absence of beads. As can be seen in Table S4, turbulent flow conditions prevailed during all experimental runs. Therefore, it was not necessary to consider the ε_{ht} term.

The granular temperature, θ, is essential for hydrodynamic descriptions (Goldhirsch, 2008). It measures the kinetic energy of the grinding medium, and therefore of the speed and number of compression events that take place in the process (Eskin et al., 2005; Goldhirsch, 2008). This microhydrodynamic parameter varied significantly ($p<0.05$) with c_S and d_b. Lower values of θ were observed with smaller beads; these are more closely packed, leading to a greater number of inelastic collisions between them, producing a greater energy dissipation, and, as a consequence, a less vigorous fluctuating movement (Afolabi et al., 2014). On the other hand, θ significantly ($p<0.05$) decreases with increasing starch concentration. This behavior is consistent with the observations of Afolabi et al. (2014), who explained that the increase in the viscosity of suspensions (see Figures 4a to c) would cause a decrease in the speed of the grinding medium.

The milling intensity factor, F, was introduced as a parameter dependent on the experimental factors (excluding the mechanical properties of starch). According to Eq. 16, the variation of any experimental factor reflects a change in F, which in turn is proportional to the variation of the energy dissipation rate due to particle deformation or Π (Eq. 14). In the present study, F varied significantly ($p<0.05$) with c_S and d_b. The observed behavior within the experimental domain is depicted in **Fig. 6a**. F increased when using larger beads. This will be explained in more detail in the next paragraph, where the effect of d_b on a (average frequency of particle compressions) and σ_b (maximum bead contact pressure) is analyzed. On the other hand, an increase in c_S produces a decay in F. This result is similar to that reported by Afolabi et al. (2014). The authors explained that by increasing the number of particles trapped between beads, the compression force applied to each individual particle decreases. Hence, the milling efficiency is reduced. In addition, it is important to point out that a significant ($p<0.05$) and positive correlation between F and k_m was observed ($r=0.8696$), highlighting that faster breakage kinetics are associated with higher intensity factors.

The maximum contact pressure between beads, $\sigma_{b,max}$, and the average frequency particle compression, a, were significantly influenced ($p<0.05$) by d_b. Li et al. (2016) found that in the range of 50-100 μm, smaller beads tend to decrease $\sigma_{b,max}$ (which is unfavorable for fracture), but to increase a (which is favorable for fracture). The overall impact of d_b will depend on which of these opposing effects predominates. The results of the present contribution suggest that the first unfavorable effect predominates when using smaller beads. Hence, lower values of F are observed with smaller beads.

On the other hand, c_S did not significantly affect $\sigma_{b,max}$ ($p>0.05$), however, an increase in starch concentration significantly ($p<0.05$) increased the parameter a. Since there are more

particles in the system, the probability of a particle being trapped between two beads increases. Despite this, the effectiveness of the compression events is reduced (Afolabi et al., 2014).

According to the behavior observed previously, it is important to highlight that if reliable values of all mechanical properties were available, the value of the λ factor could be calculated (Eq. 15), as well as the energy dissipation rate Π (Eq. 14). Eskin et al. (2005) suggested a way of calculating the milling efficiency (η), which expresses the fraction of the energy provided by the mill stirrer (P_w) that is used for the creation of new surface area (Π):

$$\eta = \frac{\Pi}{P_w} \qquad \text{(Eq. 21)}$$

Another rapid way of estimating the energy required for new surface area creation (E', J) is the following alternative form of the Rittinger's equation (Zárate, 2015):

$$E' = \frac{m_1}{k_v \rho_p} k_s \left(\frac{1}{Z_f} - \frac{1}{Z_0}\right) \qquad \text{(Eq. 22)}$$

where m_1 and ρ_p are the mass (kg) and density (1500 kg.m^{-3}) of the milled material, respectively; k_v and k_s are form factors, which are equal to π/6 and π, respectively for spherical particles.

E' values were calculated as an alternative way to estimate η without precise values of the mechanical properties, which are usually difficult to measure (Afolabi et al., 2014; Parker et al., 2020). The power P' (W) consumed for new area creation was obtained from E' and the milling operation time. Finally, the milling efficiency was estimated using an expression similar to that shown in Eq. 21:

$$\eta = \frac{P'/V_c}{P_w} \qquad \text{(Eq. 23)}$$

where V_c is the occupied volume of the milling chamber. Therefore, P'/V_c is the power consumed for new area creation per unit volume (W.m^{-3}).

All these values are shown in **Table S5** of the Supplementary Material. As can be seen in the table, only a very small fraction of the energy spent on stirring is transformed into the deformation of particles. Indeed, the calculated η values were in the range of 0.0044-0.0128. These estimated values, as function of the experimental factors, are shown in **Fig. 6b**. In this regard, Eskin et al. (2005) reported η values of the same order of magnitude (0.002-0.005), for the milling of an organic pigment in laboratory scale mill.

Although the highest milling intensity factor F was calculated for a c_S of 1% (w/v) and d_b of 0.5 mm (0.0740 m$^{2.6}$.s$^{-2.6}$, Table S4), an enhanced process efficiency η was estimated

(0.0128) for a c_S of 7% (w/v) and d_b of 0.5 mm (Table S5). Both variables (F and η) used together highlight two concluding remarks for an enhanced milling process efficiency: 1) the need of larger beads and 2) the processing of a higher mass of solids. Hence, the practical implication of the η concept introduced in Eq. 23 relies on the consideration of the mass of milled material.

3.5. Redispersible powders obtained from the spray drying of corn starch nanosuspensions.

In order to obtain redispersible powders from corn starch nanosuspensions, a spray drying process was performed. The highest c_S studied above (7% w/v) was used to increase the solid yield of the drying process. Therefore, it is important to highlight that the results of sections 3.5.1 to 3.5.4 were obtained from the spray drying of nanosuspensions prepared with a c_S of 7% (w/v), three different concentrations of SDS (0, 0.7 and 1% w/v) and a d_b of 0.15 mm. Given the enhanced milling efficiency with larger beads (discussed in section 3.4), the use of beads with a d_b of 0.5 mm for the preparation, spray drying and structural characterization of corn starch nanoparticles in powder will be analyzed in a forthcoming contribution by our group.

3.5.1. Particle size distribution.

The average particle size of parent nanosuspensions, and after being spray-dried and redispersed are given in **Table 5**. In the same table, other important properties of parent nanosuspensions such as their ζ-potential and rheological behavior are also shown.

As can be seen in **Figure 7**, the presence of surfactant in the formulation greatly ($p<0.05$) improves the dispersibility of powders, compared with native starches. These observations are in accordance with sections 3.1 and 3.3, in which the role of SDS to prevent the aggregation phenomena of particles was addressed. In this regard, it is worth pointing out that a significant ($p<0.05$) increase in Z_{av} was observed after spray drying and redispersion, compared with the parent nanosuspensions, when using 0 and 0.07% (w/v) SDS as stabilizer during milling. Indeed, the Z_{av} values of resuspended powders were above 1 μm (Table 5). On the other hand, the Z_{av} was not significantly modified ($p>0.05$) after spray drying of nanosuspensions stabilized with the largest proportion of SDS. Besides the highest ζ-potential with 1% (w/v) of SDS as stabilizer (Table 5), the increased viscosity of the system due to the enhanced swelling of starch in the presence of different proportions of SDS has been explained in section 3.2. According to Table 5, a significant ($p<0.05$) increase in the

consistency index *K*, as well as a decrease in the flow index *n* were observed with 1% (w/v) of SDS. Both the electrical charge and the enhanced viscosity might decrease the internal circulation and oscillation of droplets during atomization and prevent their re-coalescence, which might account for the stability of particle size after spray drying (Us-Medina et al., 2018). These results were also supported by TEM observations (section 3.5.4).

3.5.2. Differential scanning calorimetry.

It is known that starch granules undergo different thermal transitions when subjected to heat treatment due to their partially crystalline state. The thermal properties of starches are given in **Table 6** and the thermograms are depicted in **Figures 8 a** to **c**. The gelatinization enthalpies of native starches are generally between 5-20 $J.g^{-1}$ and greatly vary according to the nature and processing of the granules (Whistler et al., 2009). Fu et al. (2012) reported the following values for native corn starch, in accordance with Table 6 and for similar moisture contents: 12.97±0.28 $J.g^{-1}$, 63.82±0.20 °C, 68.76±0.11 °C and 73.86±0.78 °C for ΔH, T_0, T_p and T_e, respectively. The gelatinization event of native corn starch is shown in curve "A" (Fig. 8a).

After homogenization and spray drying of native starch suspensions, a small shift in T_0 was evident. The corresponding gelatinization event is shown in the B curve of Fig. 8a. However, this shift was not statistically significant ($p>0.05$) compared with native starches (Table 6). Therefore, the homogenization and drying processes applied in this study were not intense enough to significantly affect the internal structure and crystalline organization of granules. These results agree with those reported by Fu et al. (2012), who managed to keep intact the microstructure of pregelatinized starch powders after spray drying.

As a result of the milling process, starch granules become gelatinized. This latter can be seen in the curves "E" (7% (w/v) S+1% (w/v) SDS), "F" (7% (w/v) S+0.07% (w/v) SDS) and "G" (7% (w/v) S) of Fig. 8b. A similar phenomenon was observed by Lu et al. (2018) for corn starch after a milling time greater than 15 h. In gelatinized starches, which were cooled and stored, fusion of retrograded amylopectin and fusion of amylose-lipid complex phenomena are usually observed after a second heating run in DCS. On cooling, amylose and amylopectin molecules begin to reassociate. The restoration of molecular order in starch is a complex phenomenon known as retrogradation, which depends on many factors such as sources of starch, concentration, heating and cooling rates, pH, and solutes (lipid, electrolytes, sugars) (Whistler et al., 2009). In this regard, thermal analysis techniques are sensitive to the chain ordering of the amylopectin fraction, which is evidenced by a

retrogradation endotherm between 45 - 60 °C (Schmiele et al., 2019). Post-gelatinization changes could be observed after one week (retrogradation) in native starch (curve "C", Fig. 8a), in homogenized and spray-dried starches (curve "D", Fig. 8a), and in starch samples obtained via WSMM: curves "F" (7% (w/v) S+0.07% (w/v) SDS) and "G" (7% (w/v) S) of Fig. 8b. For all these samples, T_0 of retrogradation was between 46 and 51 °C. Moreover, it is worth pointing out that there was no noticeable retrogradation event (curve "E", Fig. 8b) for the starch sample formulated with the highest proportion of SDS (7% (w/v) S+1% (w/v) SDS). With the addition of SDS, the retrogradation enthalpy continually decreased (Table 6). This might be attributed to the favored formation of amylose-SDS non-retrograding complexes as the SDS concentration increased, which was mentioned in section 3.1.

Regarding the formation of amylose-lipid complexes, it is worth mentioning that they often possess significant heterogeneity in terms of aggregation and order. Usually, the peak temperature of amylose-ligand dissociation upon heating is around 80-120 °C (Di Marco et al., 2024). Two polymorphs have been well described: type I (melting temperature at around 90-105 °C) and type II (melting temperature at around 115-130 °C). The final polymorph will depend on the temperature, annealing time, and ligand type (Hay et al., 2019; Sun et al., 2021). Type I is a random distribution of helical elements formed by rapid nucleation as a consequence of low crystallization temperatures. On the other hand, type II has been described as composed of crystalline lamellar structures, obtained at higher crystallization temperatures or by conversion of type I by partial melting and recrystallization (Kong et al., 2019; Sun et al., 2021).

In the present contribution, the T_p observed for the amylose-SDS complex dissociation (curves "E" and "F", Fig. 8b) was around 90 °C (Table 6), with no significant differences ($p>0.05$) between the added proportion of SDS. According to these results, the formation of polymorph I was promoted. At low temperatures, (<60 °C) the nucleation rate is high, which may favor a rapid and random freezing of the helical segments (Di Marco et al., 2024). Therefore, the temperature conditions during milling and storage of nanosuspensions before spray drying may promote the formation of polymorphs with a lower T_p. On the other hand, at higher temperatures (>90 °C) the nucleation rate is low, and the complexation progresses like a conventional crystallization process. As a consequence, more ordered structures with a higher T_p are obtained (Di Marco et al., 2024). These results confirmed that amylose-SDS complexes were formed, which exhibit enhanced solubility and emulsifying capacity compared with native starches (Hay et al., 2019). In turn, these observations support the particle size results discussed in section 3.5.1.

Curiously, two endotherms were also observed within the above temperature range (80-120 °C) in the starch sample obtained by milling in the absence of SDS (7% (w/v) S). These could be seen in curve "G" (Fig. 8b). Besides emulsifiers, monoglycerides, fatty acids and linear alcohols, internal starch lipids may also form complexes with amylose (Whistler et al., 2009). The dissociation of these complexes with internal starch lipids might account for the endotherm around 90 °C in curve "G". In this regard, as explained for the other starch samples obtained via WSMM, the milling temperature conditions might promote the formation of polymorph I. Moreover, the other endotherm observed with a T_p around 110 °C could be attributed to the formation of polymorph II.

Finally, the thermogram of pure SDS is also shown (curve "H", Fig. 8c) in the same temperature range of the other samples. Two endotherms were observed, which might be accounted for by a fusion of ionic bilayers. This thermal process might involve two endotherms either due to relative stability, size and accessibility of surfactant molecules (Di Battista, 2016; Makowska et al., 2015). These endotherms were not observed in the thermograms of starch samples obtained via WSMM (Figure 8b). Therefore, from the comparison of thermograms in Figures 8a, b and c, it could be concluded that new complexes between starch components and SDS were effectively formed.

3.5.3. *X-ray diffraction.*

The X-ray diffraction patterns of powders are shown in **Figures 9a** to **b**. Regarding the starch samples, curves "A" and "B" correspond to native starch, and homogenized and spray-dried starch, respectively. As can be seen, the homogenization and spray drying processes did not alter the crystallinity of starch, in accordance with the thermograms discussed in the previous section. The relative crystallinity percentages were 43.62% and 47.54% for native starch, and for homogenized and spray-dried starch, respectively. Both samples exhibited the A-type pattern with defined peaks at 15.09°, 17.04°, 18.02°, 19.97° and 23.18° (2θ), in accordance with Piloni et al. (2022) for corn starch.

The milling process promoted the formation of other crystal types. For instance, curve "C" in Fig. 9a corresponds to the starch sample obtained via WSMM in the absence of SDS (7% (w/v) S). As a consequence of the milling process, the relative crystallinity percentage was reduced (40.54%). In accordance with the thermograms discussed in the previous section, some characteristic peaks of the B-type pattern were observed in the sample: 12.48°, 17.1°, 20.76° (2θ) (Buleón et al., 1998)). On the other hand, as the surfactant concentration increased, the relative crystallinity percentage decreased further: 22.02% (7% (w/v) S+0.07%

(w/v) SDS, curve "D", Fig. 9a) and 4.32% (7% (w/v) S+1% (w/v) SDS, curve "E", Fig. 9a). Moreover, characteristic peaks of the V-type appeared. In curve "D", defined peaks at 12.84° and 19.52° (2θ) were identified. According to Hay et al. (2019) and Di Marco et al. (2024), this pattern indicates the presence of helical amylose inclusion complexes, with six units per turn. The 6_1V type is a tightly packed crystalline unit cell, which lacks sufficient interstitial space for any guest molecule to reside (Hay et al., 2019). Regarding curve "E", a broad amorphous hallo predominates in this sample, in accordance with Patel et al. (2016). It has been well described that the WSMM process generally reduces the crystallinity of materials, and when the particle size decreases, so does the intensity of the diffraction peaks (Patel et al., 2016). In this regard, according to Table 5, the addition of surfactant helped reduce the particle size, and so did the intensity of the diffraction peaks.

Finally, curve "F" in Fig. 9b corresponds to pure SDS. This diffraction pattern evidenced the presence of a solid with a high crystallinity, given the multiplicity of well defined peaks. Moreover, this pattern was in agreement with the reports of Chantraine et al. (2007) for SDS in powder.

In accordance with section 3.5.2, the original diffraction peaks of SDS were not present in the diffractograms of the starch samples obtained via WSMM, which supports the formation of new complexes between starch components and SDS during milling.

3.5.4. *Transmission electron microscopy.*

Figures 10a to **h** show the morphological features and particle size of all starch samples. Corn starch granules (Figs. 10a, b) showed the characteristic truncated shape of native corn starch (Fu et al., 2012). As a consequence of the milling operation, the main feature observed was the occurrence of less electron-dense particles, compared with the native starch, reflecting a mechanical damage to the native granules. After spray drying of the parent nanosuspensions, and resuspension of the obtained powders, the particle size distribution was remarkably changed compared with the sizes recorded immediately after milling, depending on the proportion of SDS used as stabilizer.

As the concentration of SDS increased, the average particle size and the PDI decreased, which was evidenced in Figs. 10c, e and g. These observations were in accordance with the DLS measurements shown in Table 5. Among the starch samples prepared via WSMM and subsequent drying, the polydispersity of particles was noticeable in the absence of stabilizer. In addition, for the studied milling conditions (starch concentration of 7% w/v and bead diameter of 0.15 mm) the use of 0 and 0.07% (w/v) of SDS as a stabilizer could not have

been enough to prevent reaggregation of the atomized droplets during atomization, leading to particle sizes above 1 μm (Figs. 10c to f).

The internal structure of granules was significantly modified after the milling process (Patel et al., 2016; Zhu et al., 2020). With subsequent spray drying, non spherical and shrunken particles were especially evident for 7% (w/v) S (Figs. 10c, d) and 7% (w/v) S + 0.07% (w/v) SDS (Figs. 10e, f) samples. In addition, it is worth pointing out that the morphology observed in starches obtained via WSMM was similar to that reported by Fu et al. (2012) for pregelatinized starches. The development of rough surfaces in gelatinized starch particles after milling could be due to the high moisture gradients between the drying-air and the inner part of droplets/particles (Fu et al., 2012).

On the other hand, nanoparticles could be obtained after the spray drying of nanosuspensions stabilized with 1% (w/v) of SDS during milling (Figs. 10g, h). Moreover, gel-like structures around particles were observed in the presence of SDS (Figs. 10e to h), evidencing the enhanced swelling of starch due to this surfactant (Svensson et al., 1998). With the largest proportion of SDS, the granular shape was totally lost and the granules were fully fragmented, supporting the conclusions given by the X-ray patterns (section 3.5.3). Tiny and non-aggregated particles with irregular edges were observed (Figs. 10g, h), which was also informed by Bajer et al. (2023) and Liu et al. (2018) for starch nanoparticles developed via acid hydrolysis and ultrasound treatments, and ultrasonic treatment alone, respectively.

Finally, depending on the proportion of SDS used during milling, micro or nanoparticles could be obtained from the spray drying of nanosuspensions. The above results suggest that the addition of a stabilizer does not only prevent particle reaggregation during milling, but also during drying operations applied for the conservation of starch nanoparticles. This latter is of utmost importance to facilitate the transport and subsequent use of these particles, especially as Pickering emulsifiers (Di Giorgio et al., 2020).

4. Conclusion.

In the above study, the wet-stirred media milling process (WSMM) was systematically analyzed for the development of physically stable corn starch nanosuspensions. The preliminary analysis performed with 1% (w/v) of starch revealed that the correct use of surfactants (SDS) and post-milling operations such as centrifugation and homogenization yielded stable nanoparticles with Z_{av} = 161±5 nm, starting from an initial average particle size of 14.08±0.08 μm. In this regard, the use of SDS prevented particle aggregation during

milling and allowed the formation of new amylose-SDS complexes, which was mainly evidenced by DSC and X-ray diffraction techniques.

The multiple response optimization study, the breakage kinetics and the microhydrodynamic analysis showed that the use of larger beads (average diameter of 0.50 mm against 0.15 mm) and lower starch concentrations (around 1-2% w/v) improved the WSMM process. On the one hand, increasing the number of suspended particles causes a decrease in the compression force applied to each individual particle. On the other hand, the intensity of collisions predominates over their frequency when working with larger zirconia beads. Therefore, higher values of the apparent breakage rate constant (k_m) and of the milling intensity factor (F) were observed.

The milling efficiency (η) was also calculated. Only a small fraction of the energy spent on stirring is transformed into the deformation of particles, and the highest η value was calculated for a c_S of 7% (w/v), which allows the processing of a higher solid content. In accordance with the optimization study, kinetic and microhydrodynamic analysis, enhanced η values were observed with larger zirconia beads.

Finally, corn starch micro and nanoparticles were obtained upon spray drying of nanosuspensions formulated with a c_S of 7% (w/v) and different proportions of SDS as a stabilizer during milling. TEM and X-ray diffraction techniques helped confirm the full fragmentation of granules with 1% (w/v) of SDS and the formation of nanoparticles even after spray drying and resuspension. These particles showed an enhanced redispersion, compared with native starch.

The above promising results clearly showed that the WSMM process could be implemented as a solvent-free methodology to obtain nanoparticles derived from biopolymers, which are able to deliver a wide myriad of bioactive compounds. Therefore, the synthesis of nanosuspensions with larger beads (0.50 mm), their storage stability after spray drying, their emulsifying behavior in Pickering emulsions, and their interfacial properties at the O/W interface will be studied in two forthcoming publications by our research group.

Declaration of competing interests.

The authors declare no conflict of interest.

Acknowledgements.

This work was supported by grants from Ia ValSe-Food-CYTED (119RT0567), MinCyT-PIO Bio (Decreto Nº 349/2022-Res. Mi. Nº 00000043/2022), CONICET (PIP 2021–2023 11220200102830CO), ANPCyT (PICT 2019-01122), and SeCyT-UNC, Córdoba, Argentina.

References

AACC, 2000. Approved Methods of the American Association of Cereal Chemists, 10th ed. St. Paul, MN, USA: The Association.

Afolabi, A., Akinlabi, O., Bilgili, E., 2014. Impact of process parameters on the breakage kinetics of poorly water-soluble drugs during wet stirred media milling: A microhydrodynamic view. Eur J Pharm Sci. 51, 75-86.

Ahmad, M., Gani, A., Hassan, I., Huang, Q., Shabbir, H., 2020. Production and characterization of starch nanoparticles by mild alkali hydrolysis and ultra-sonication process. Sci Rep. 10(1), 3533.

Albert, C., Beladjine, M., Tsapis, N., Fattal, E., Agnely, F., Huang, N., 2019. Pickering emulsions: Preparation processes, key parameters governing their properties and potential for pharmaceutical applications. J Control Release. 309, 302-332.

Amparo, L.R., Rovira, M.J.F., Sanz, M.M., Gomez-Mascaraque, L.G. 2018, Nanomaterials for food applications, Elsevier.

Azad, M., Guner, G., Afolabi, A., Davé, R., Bilgili, E., 2021. Impact of solvents during wet stirred media milling of cross-linked biopolymer suspensions. Adv Powder Technol. 32(12), 4562-4575.

Bajer, D., 2023. Nano-starch for food applications obtained by hydrolysis and ultrasonication methods. Food Chem. 402, 134489.

Bhakay, A., Rahman, M., Dave, R. N., & Bilgili, E., 2018. Bioavailability enhancement of poorly water-soluble drugs via nanocomposites: Formulation–Processing aspects and challenges. Pharmaceutics. 10(3), 86.

Biliaderis, C.G., 2009. Structural Transitions and Related Physical Properties of Starch. In: B.M. James and W. Roy (Eds.), Starch: Chemistry and Technology, 3rd Edition, Academic Press, U.K., pp. 293-359.

Bordón, M. G., Paredes, A. J., Camacho, N. M., Penci, M. C., González, A., Palma, S. D., Ribotta, P.D., Martinez, M. L., 2021a. Formulation, spray-drying and physicochemical characterization of functional powders loaded with chia seed oil and prepared by complex coacervation. Powder Technol. 391, 479-493.

Bordón, M. G., Alasino, N. P. X., Villanueva-Lazo, Á., Carrera-Sánchez, C., Pedroche-Jiménez, J., del Carmen Millán-Linares, M., Ribotta, P.D., Martínez, M. L., 2021b. Scale-up and optimization of the spray drying conditions for the development of functional microparticles based on chia oil. Food Bioprod Process. 130, 48-67.

Buleón, A., Colonna, P., Planchot, V., Ball, S., 1998. Starch granules: structure and biosynthesis. Int J Biol Macromol. 23(2), 85-112.

Chantraine, F., Viana, M., Cazalbou, S., Brielles, N., Mondain-Monval, O., Pouget, C., Branlard, P., Chulia, D., 2007. From compressibility to structural investigation of sodium dodecyl sulphate—Part 2: A singular behavior under pressure. Powder Technol. 177(1), 41-50.

Chen, C. J., Shen, Y. C., Yeh, A. I., 2010. Physico-chemical characteristics of media-milled corn starch. J Agric Food Chem. 58(16), 9083-9091.

Di Battista, C.A., 2016. Microencapsulación de fitoesteroles mediante secado por atomización, Tesis de Doctor en Ingeniería Química, Universidad Nacional del Sur.

Di Giorgio, L., Martín, L., Salgado, P. R., Mauri, A. N., 2020. Synthesis and conservation of cellulose nanocrystals. Carbohydr Polym. 238, 116187.

Di Marco, A. E., Tomás, M. C., Ixtaina, V. Y., 2024. Improved accelerated stability of starch-chia oil fatty acid inclusion complexes formed under mild reaction conditions. Carbohydr Polym. 331, 121887.

Doran, P. M, 1995. Bioprocess engineering principles, Elsevier.

Dubey, R., Toh, Y. R., Yeh, A. I., 2018. Enhancing cellulose functionalities by size reduction using media-mill. Sci Rep. 8(1), 11343.

Eskin, D., Zhupanska, O., Hamey, R., Moudgil, B., Scarlett, B., 2005. Microhydrodynamic analysis of nanogrinding in stirred media mills. AIChE Journal. 51(5), 1346-1358.

Flach, F., Breitung-Faes, S., Kwade, A., 2018. Model based process optimization of nanosuspension preparation via wet stirred media milling. Powder Technol. 331, 146-154.

Food and Drug Administration (FDA). 2024. Title 21—Food and Drugs. Chapter I—Food and Drug Administration. Department of Health and Human Services. Subchapter B—Food for Human Consumption. Part 172—Food additives permitted for direct addition to food for human consumption. Subpart I—Multipurpose additives. Sec. 172.822 Sodium lauryl sulfate. CFR - Code of Federal Regulations Title 21 (fda.gov) (Last accessed 9.10.2024).

Fu, Z. Q., Wang, L. J., Li, D., Adhikari, B., 2012. Effects of partial gelatinization on structure and thermal properties of corn starch after spray drying. Carbohydr Polym. 88(4), 1319-1325.

Gibson, T.S., Solah, V.A., McCleary, B.V., 1997. A procedure to measure amylose in cereal starches and flours with concanavalin A. J Cereal Sci. 25, 111–119.

Goldhirsch, I., 2008. Introduction to granular temperature. Powder Technol. 182(2), 130-136.

Hay, W. T., Fanta, G. F., Felker, F. C., Peterson, S. C., Skory, C. D., Hojilla-Evangelista, M. P., Biresaw, G., Selling, G. W., 2019. Emulsification properties of amylose-fatty sodium salt inclusion complexes. Food Hydrocoll. 90, 490-499.

He, R., Pan, Y. G., Shang, W. T., Zhong, G., Huang, W. Y., Xiang, D., Pan, F., Zhang, W. M., 2023. Ultrasonic-assisted binding of canistel (Lucuma nervosa A. DC) seed starch with quercetin. Ultrason Sonochem. 96, 106417.

Jiang, H., Sheng, Y., Ngai, T., 2020. Pickering emulsions: Versatility of colloidal particles and recent applications. Curr Opin Colloid Interface Sci. 49, 1-15.

Kong, L., Bhosale, R., Ziegler, G. R., 2018. Encapsulation and stabilization of β-carotene by amylose inclusion complexes. Food Res Int. 105, 446-452.

Kong, L., Perez-Santos, D. M., Ziegler, G. R., 2019. Effect of guest structure on amylose-guest inclusion complexation. Food Hydrocoll. 97, 105188.

Krishna S., Patel, C. M., 2020. Computational and experimental study of mechanical properties of Nylon 6 nanocomposites reinforced with nanomilled cellulose. Mech Mater. 143, 103318.

Krishna, S., Sreedhar, I., Patel, C. M., 2023. Optimized nanomilling of biomaterials by wet-stirred media milling for efficient preparation of nanoparticles. Waste Biomass Valori. 14(2), 655-661.

Kwade, A., 2003. A stressing model for the description and optimization of grinding processes. Chem Eng Technol. 26(2), 199-205.

Li, M., Azad, M., Davé, R., Bilgili, E., 2016. Nanomilling of drugs for bioavailability enhancement: a holistic formulation-process perspective. Pharmaceutics. 8(2), 17.

Liu, C., Li, M., Ji, N., Liu, J., Xiong, L., Sun, Q., 2017. Morphology and characteristics of starch nanoparticles self-assembled via a rapid ultrasonication method for peppermint oil encapsulation. J Agric Food Chem. 65(38), 8363-8373.

Lu, X., Xiao, J., Huang, Q., 2018. Pickering emulsions stabilized by media-milled starch particles. Food Res Int. 105, 140-149.

Makowska, J., Wyrzykowski, D., Pilarski, B., Chmurzyński, L., 2015. Thermodynamics of sodium dodecyl sulphate (SDS) micellization in the presence of some biologically relevant pH buffers. J Therm Anal Calorim. 121, 257-261.

Martínez, M. L., Marín, M. A., Faller, C. M. S., Revol, J., Penci, M. C., Ribotta, P. D., 2012. Chia (Salvia hispanica L.) oil extraction: Study of processing parameters. LWT-Food Sci Technol. 47(1), 78-82.

Martínez, M. L., Bordón, M. G., Lallana, R. L., Ribotta, P. D., Maestri, D. M., 2017. Optimization of sesame oil extraction by screw-pressing at low temperature. Food Bioprocess Tech. 10, 1113-1121.

Paredes, A. J., Camacho, N. M., Schofs, L., Dib, A., del Pilar Zarazaga, M., Litterio, N., Allemandi, D.A., Sánchez Bruni, S., Lanusse, C., Palma, S. D., 2020. Ricobendazole nanocrystals obtained by media milling and spray drying: pharmacokinetic comparison with the micronized form of the drug. Int J Pharm. 585, 119501.

Parker, N., Rahman, M., Bilgili, E., 2020. Impact of media material and process parameters on breakage kinetics–energy consumption during wet media milling of drugs. Eur J Pharm Biopharm. 153, 52-67.

Patel, C. M., Chakraborty, M., Murthy, Z. V. P., 2016. Fast and scalable preparation of starch nanoparticles by stirred media milling. Adv Powder Technol. 27(4), 1287-1294.

Piloni, R. V., Bordón, M. G., Barrera, G. N., Martínez, M. L., Ribotta, P. D., 2022. Porous microparticles of corn starch as bio-carriers for chia oil. Foods. 11(24), 4022.

Putseys, J. A., Lamberts, L., Delcour, A. J., 2010. Amylose-inclusion complexes: Formation, identity and physico-chemical properties. J Cereal Sci. 51(3), 238-247.

Rostamabadi, H., Bajer, D., Demirkesen, I., Kumar, Y., Su, C., Wang, Y., ... , Falsafi, S. R., 2023. Starch modification through its combination with other molecules: Gums, mucilages, polyphenols and salts. Carbohydr Polym. 314, 120905.

Schmiele, M., Marques Sampaio, U., Pedrosa Silva Clerici, M.T. 2019, Starches for food application: Chemical, technological and health properties, First Ed., U.S, Academic Press.

Schultz, S., Wagner, G., Urban, K., Ulrich, J., 2004. High-pressure homogenization as a process for emulsion formation. Chem Eng Technol. 27(4), 361-368.

STATGRAPHICS® Centurion XVI, 2010. STATGRAPHICS® Centurion XVI User Manual, Statpoint Technologies, Warrenton, VA, USA.

Sui, Z., & Kong, X. 2018, Physical modifications of starch, First Ed., Singapore, Springer.

Sun, S., Jin, Y., Hong, Y., Gu, Z., Cheng, L., Li, Z., Li, C., 2021. Effects of fatty acids with various chain lengths and degrees of unsaturation on the structure, physicochemical properties and digestibility of maize starch-fatty acid complexes. Food Hydrocoll. 110, 106224.

Svensson, E., Autio, K., Eliasson, A. C., 1998. The effect of sodium dodecylsulfate on gelatinization and gelation properties of wheat and potato starches. Food Hydrocoll. 12(2), 151-158.

Tatsumi, S., Murayama, Y., Hayakawa, H., Sano, M., 2009. Experimental study on the kinetics of granular gases under microgravity. J Fluid Mech. 641, 521-539.

Us-Medina, U., Julio, L. M., Segura-Campos, M. R., Ixtaina, V. Y., Tomás, M. C., 2018. Development and characterization of spray-dried chia oil microcapsules using by-products from chia as wall material. Powder Technol. 334, 1-8.

Whistler, R.L., BeMiller, J.N., Paschall, E.F., 2009. Starch: chemistry and technology, Third Ed., Academic Press.

Wu, J., Ma, G. H., 2016. Recent studies of Pickering emulsions: particles make the difference. Small. 12(34), 4633-4648.

Xu, T., Yang, J., Hua, S., Hong, Y., Gu, Z., Cheng, L., Li, Z., Li, C., 2020. Characteristics of starch-based Pickering emulsions from the interface perspective. Trends Food Sci Technol. 105, 334-346.

Zapata, F., 2021. Motor jaula de ardilla. Available online: Motor jaula de ardilla: funcionamiento, aplicaciones, ventajas (lifeder.com) (last accessed May 2024).

Zárate, C.D., 2015. Reducción de tamaño: Molinos. Available online: https://docplayer.es/9345817-Capitulo-9-reduccionde-tamano-molinos.html#google_vignette (last accessed May 2024).

Zhang, Q., Kim, D., Li, L., Patel, S., Duhamel, J., 2019. Surfactant structure-dependent interactions with modified starch nanoparticles probed by fluorescence spectroscopy. Langmuir. 35(9), 3432-3444.

Zhang, W., Zhang, J., Xia, W., 2012. The preparation of chitosan nanoparticles by wet media milling. Int J Food Sci Technol. 47(11), 2266-2272.

Zhu, W., Zheng, F., Song, X., Ren, H., Gong, H., 2020. Influence of formulation parameters on lipid oxidative stability of Pickering emulsion stabilized by hydrophobically modified starch particles. Carbohydr Polym. 246, 116649.

Figure Captions.

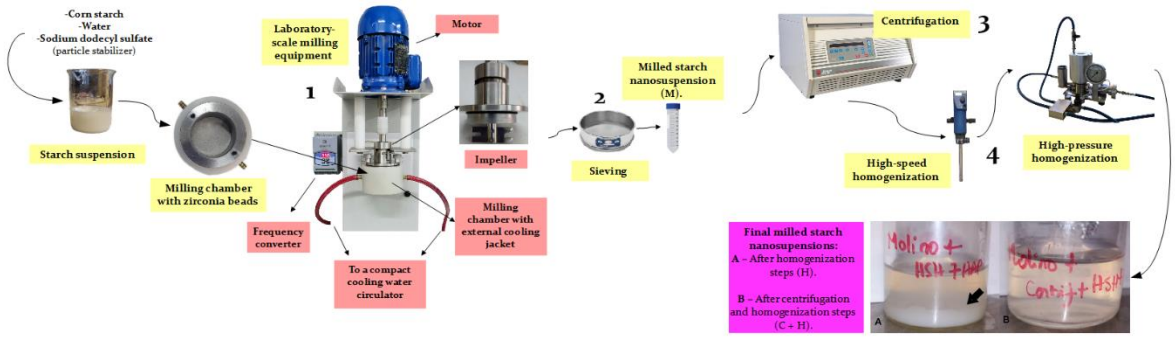

Figure 1. Wet-stirred media milling process (WSMM) and post-milling operations. The milled starch nanosupension (M) was obtained by milling (1) and separating the beads with a sieve (2). The subsequent post-milling operations studied were centrifugation (C) (3) and homogenization (H) of the supernatant (4). Moreover, the latter step consisted of high-speed homogenization followed by high-pressure homogenization.

This figure also shows starch nanosuspensions (1% w/v) stored during one week. Sedimented particles are highlighted in slide **A**, with only a homogenization step.

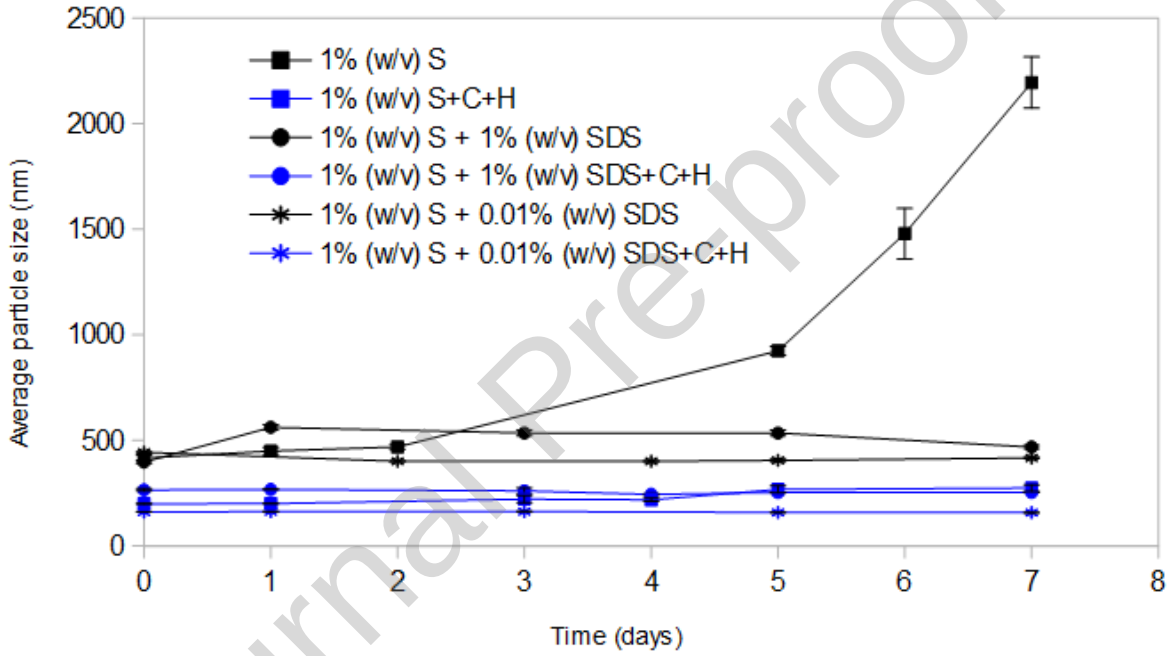

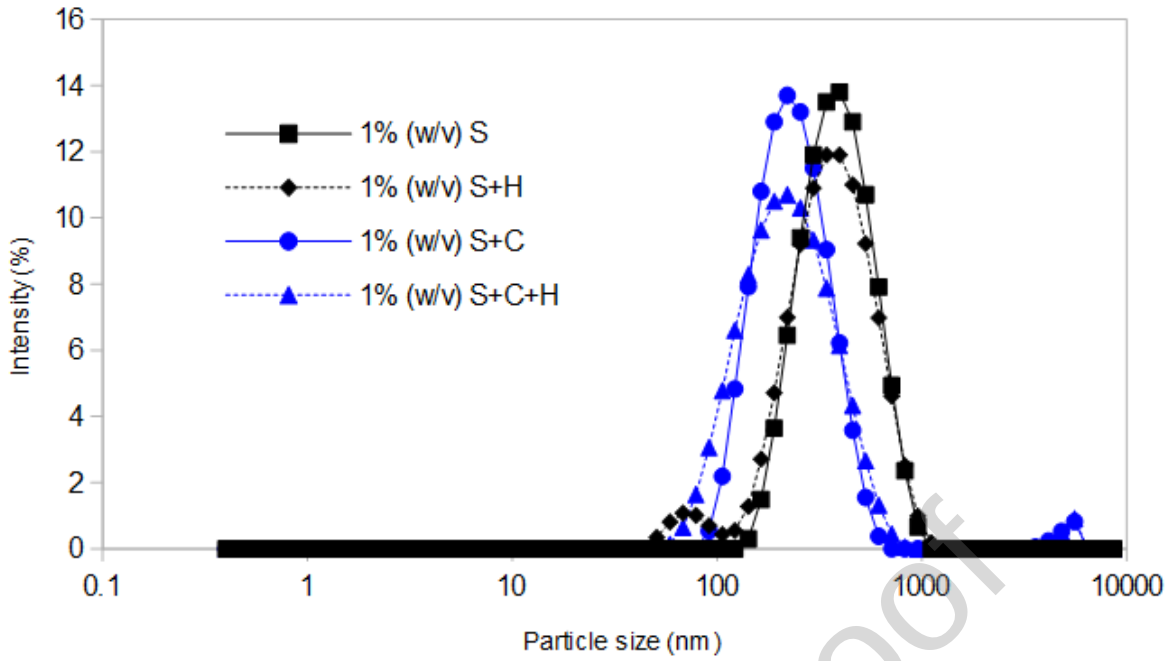

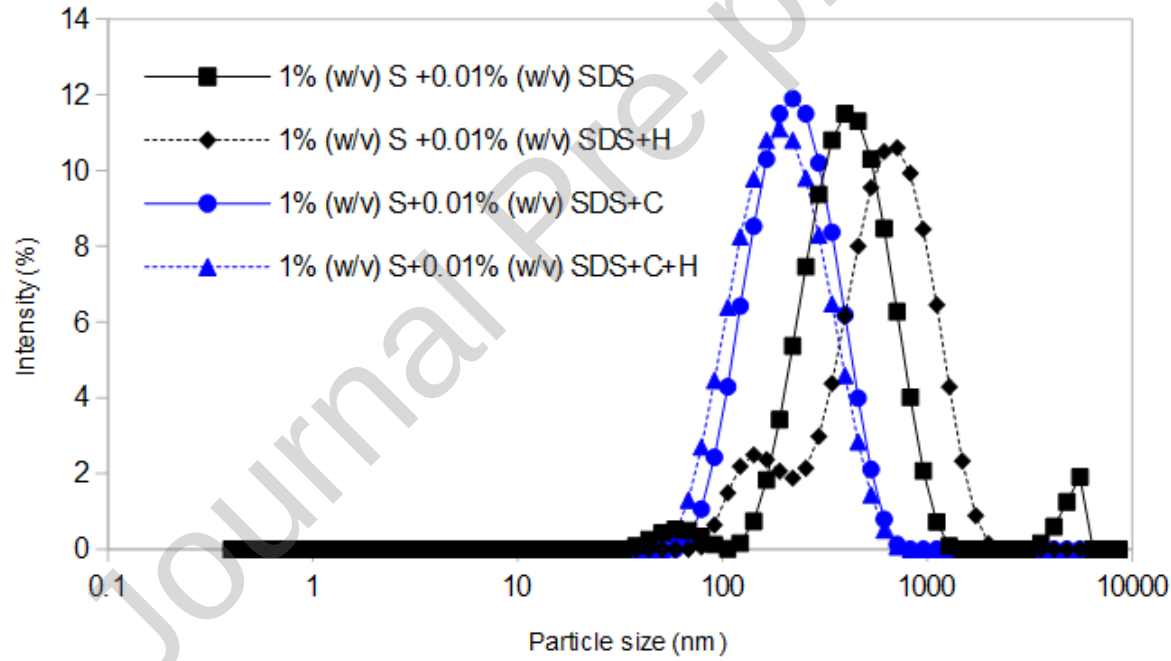

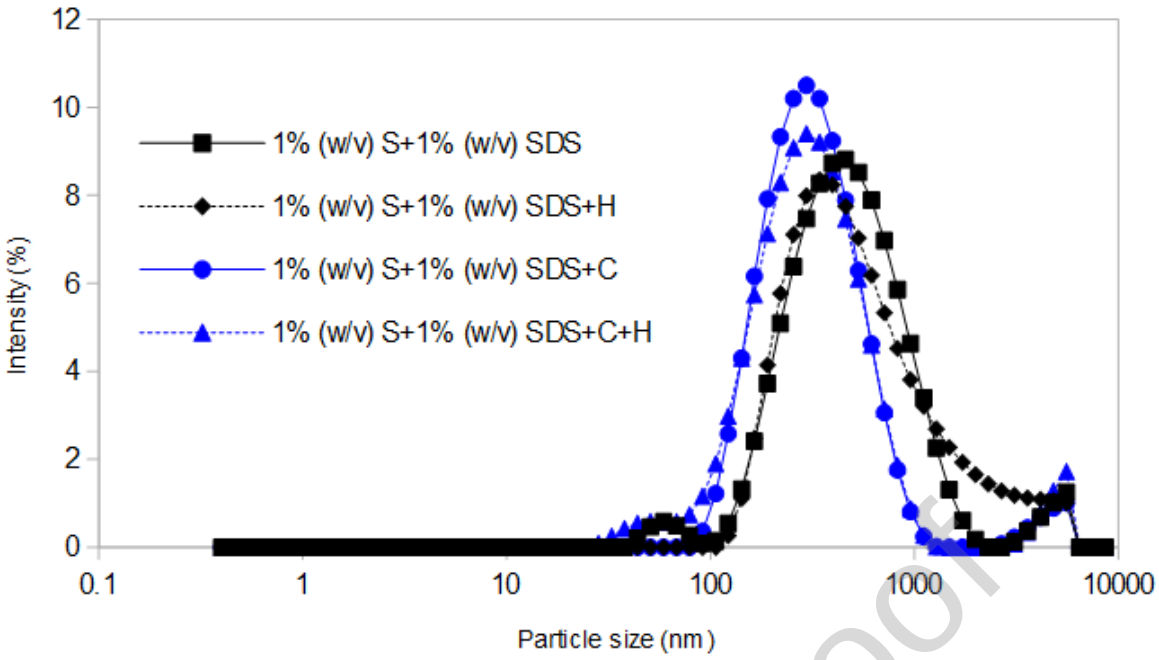

Figure 2. Particle size of corn starch nanosuspensions (1% w/v S); **a)** average particle size during storage for one week; size distributions: **b)** 0% (w/v) SDS; **c)** 0.01% (w/v) SDS; **d)** 1% (w/v) SDS. "S", "H" and "C" are "starch", "homogenization" and "centrifugation", respectively.

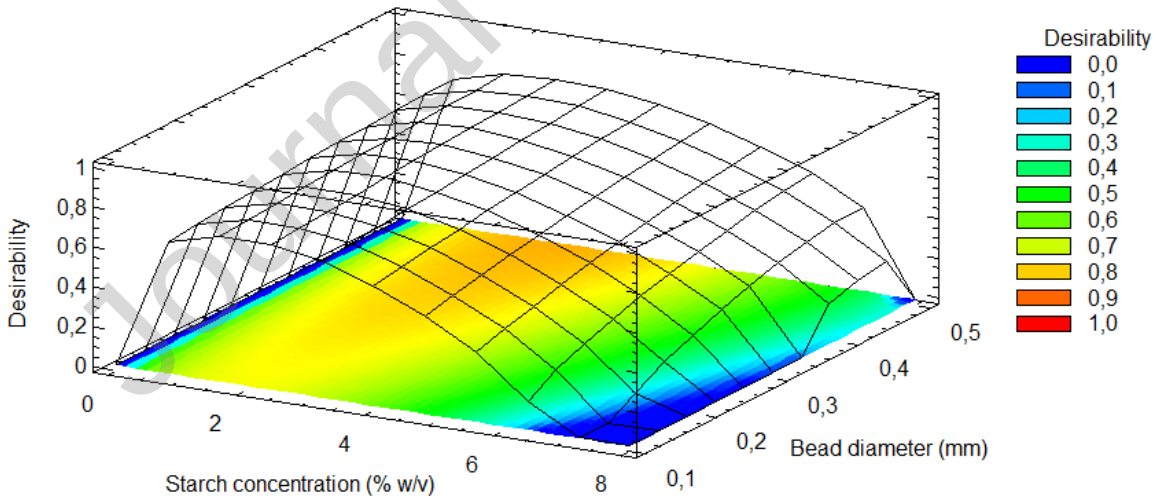

Figure 3. Estimated response surface plot of the global desirability function, for the milling process optimization.

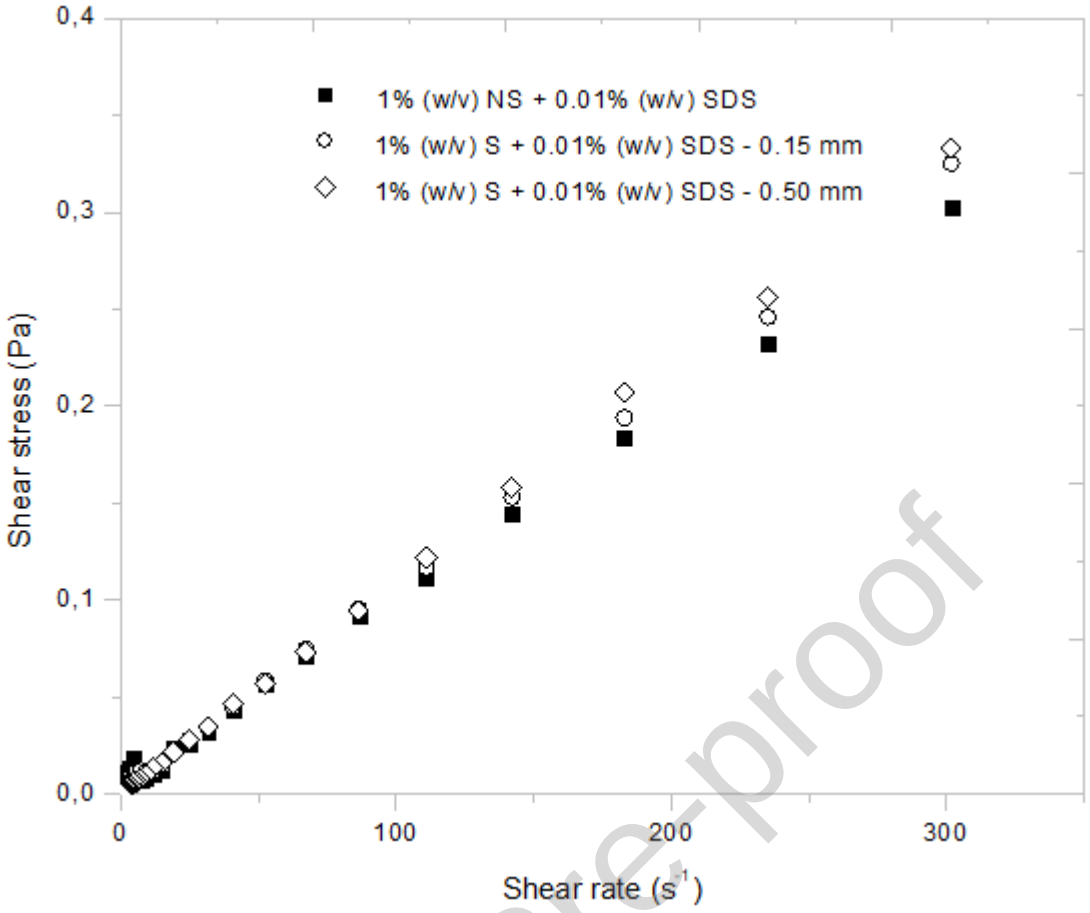

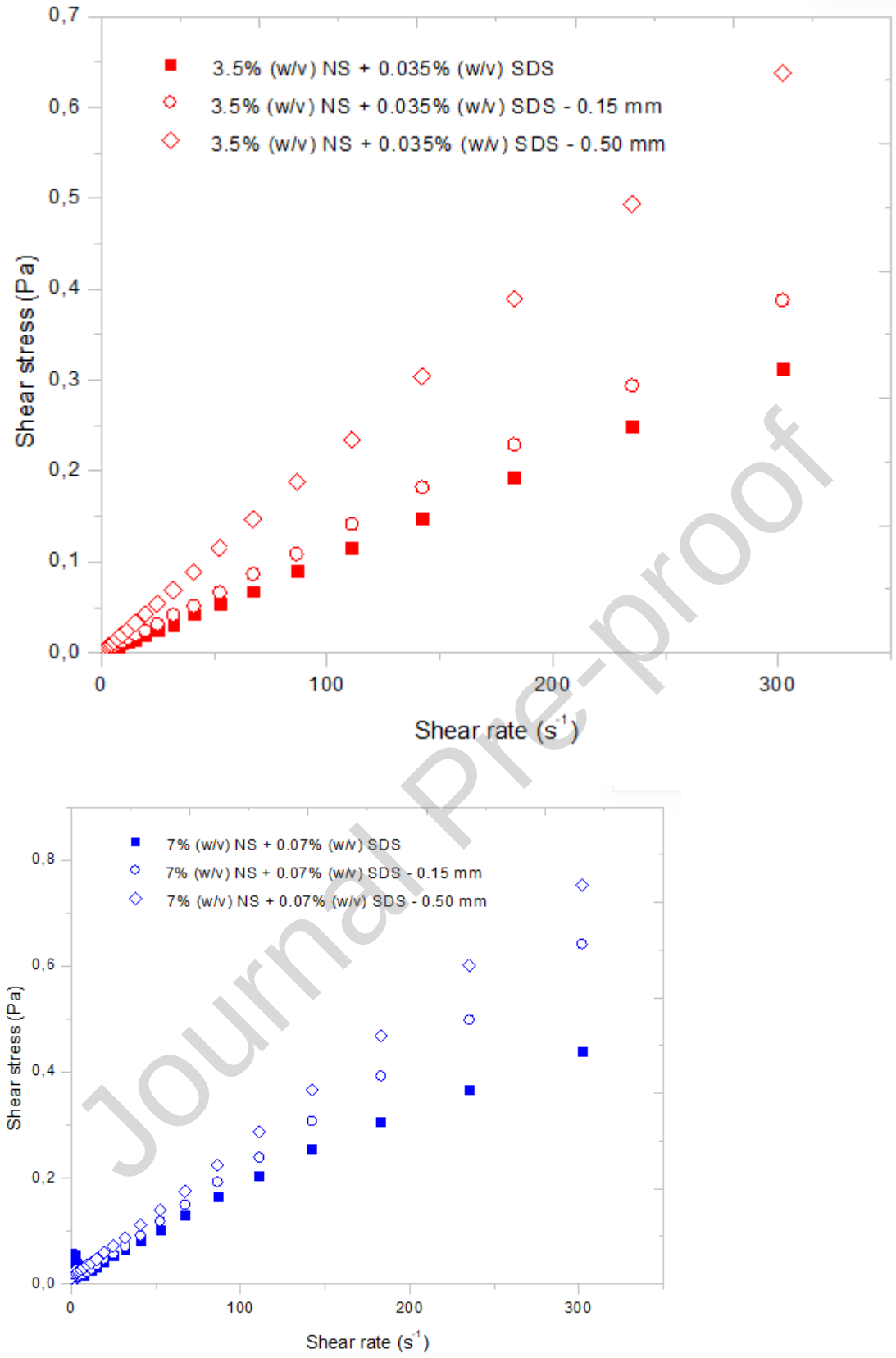

Figure 4. Rheological behavior of parent native starch suspensions (NS), and of nanosuspensions after milling. Each process condition is expressed as a combination of starch concentration (% w/v S), SDS concentration (% w/v SDS) and the average bead diameter (mm).

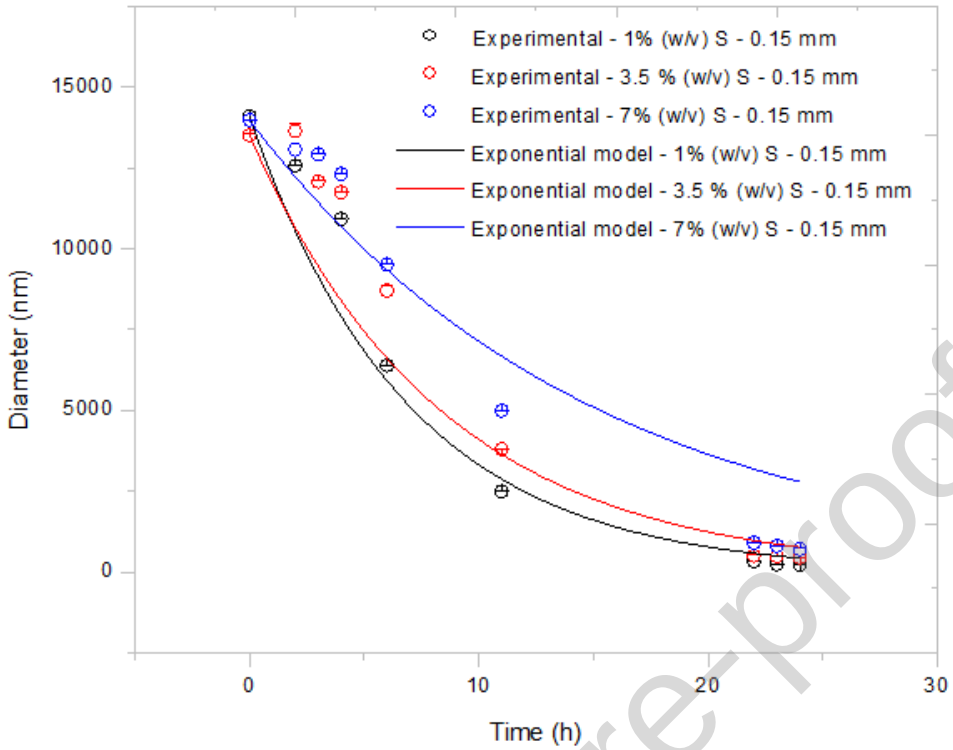

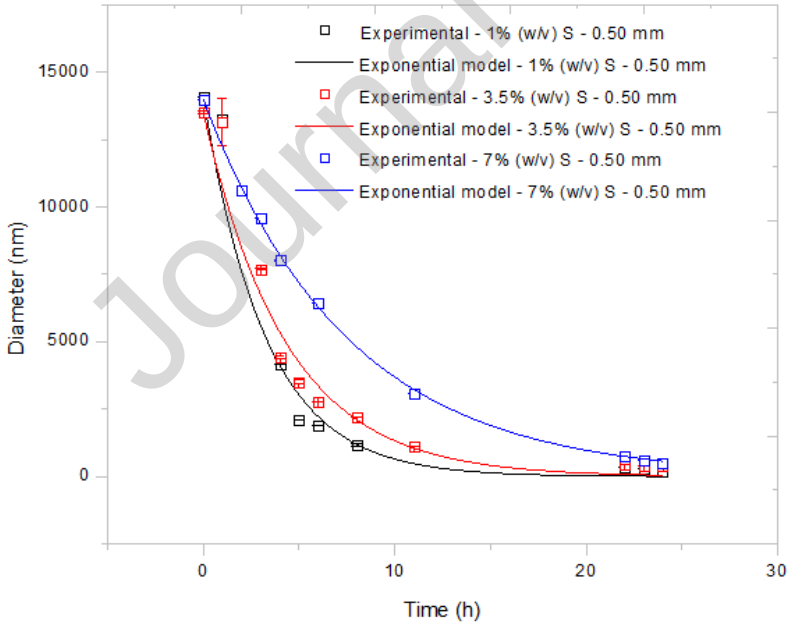

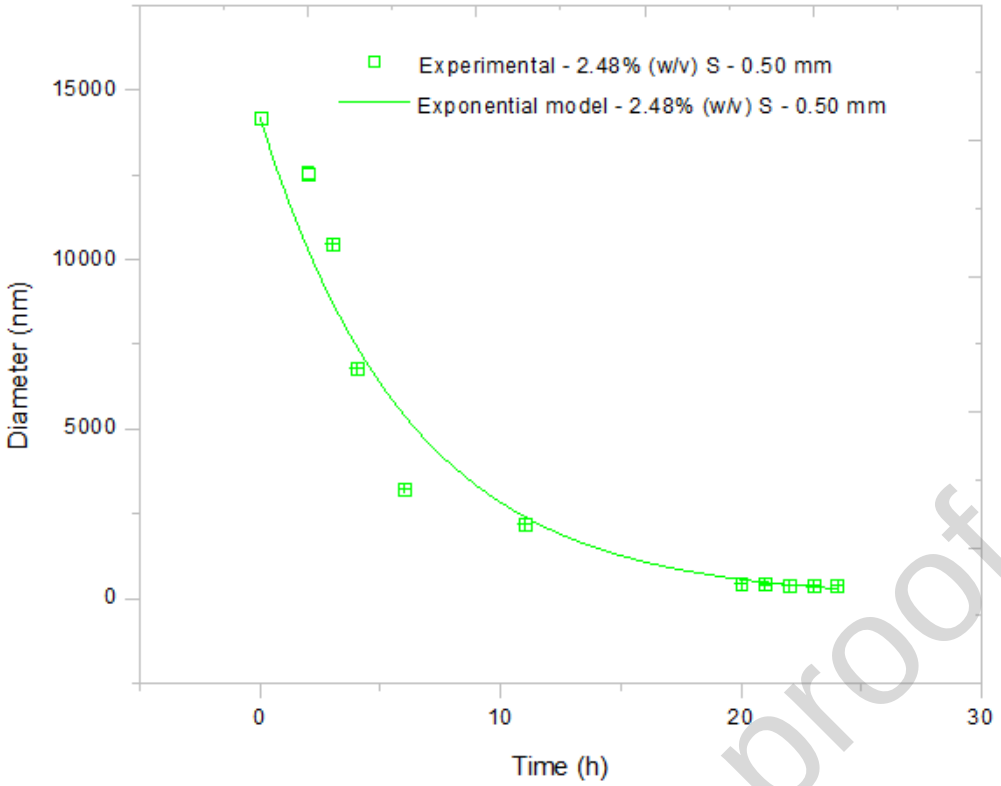

Figure 5. Breakage kinetics during milling experiments, for different combinations of corn starch (% w/v S) and average bead diameter (mm); **a)** experiments performed with a bead diameter of 0.15 mm; **b)** experiments performed with a bead diameter of 0.50 mm; **c)** experiment performed with the optimal process condition.

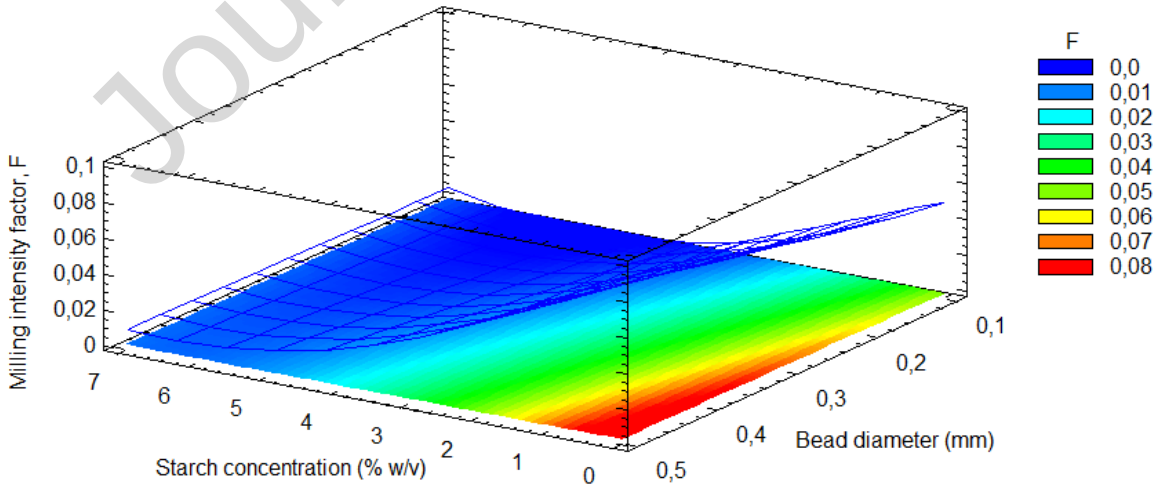

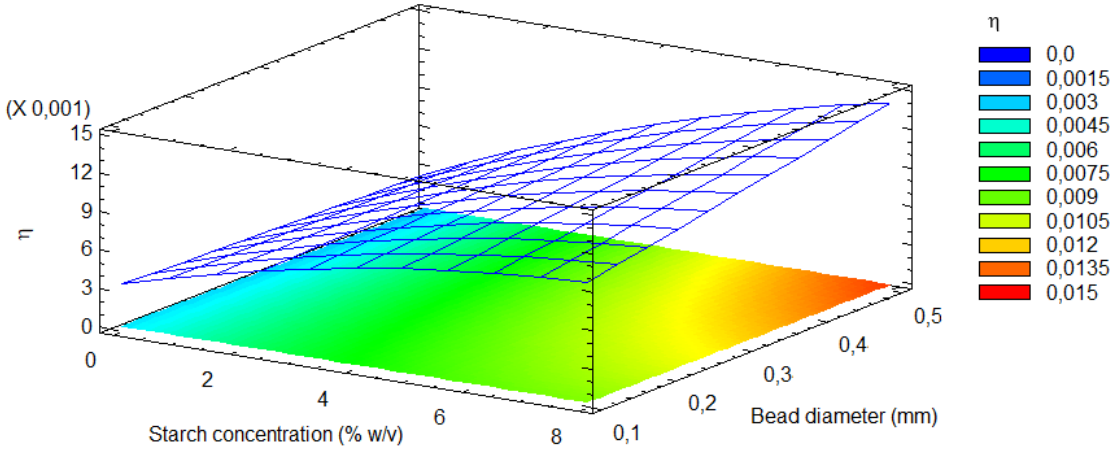

Figure 6. Response surface plots for the estimated **a)** milling intensity factor F ($m^{2.6}.s^{-2.6}$) and **b)** milling efficiency η.

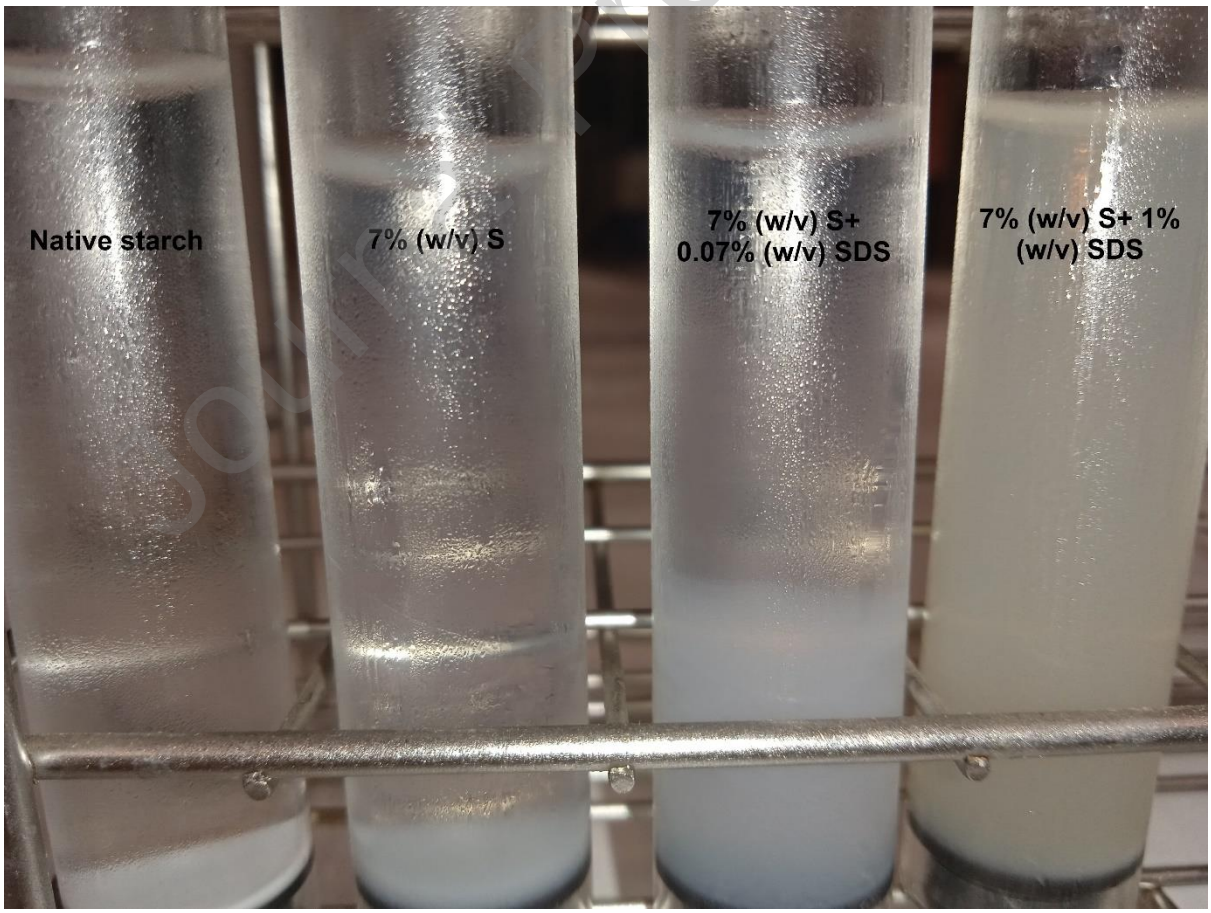

Figure 7. Physical appearance of redispersed powders after storage at 4 °C, including native starch, and starch samples obtained via WSMM and spray drying. The parent

nanosuspensions were prepared under these conditions: starch concentration (7% w/v), SDS concentration (0, 0.07, 1% w/v), bead diameter (0.15 mm).

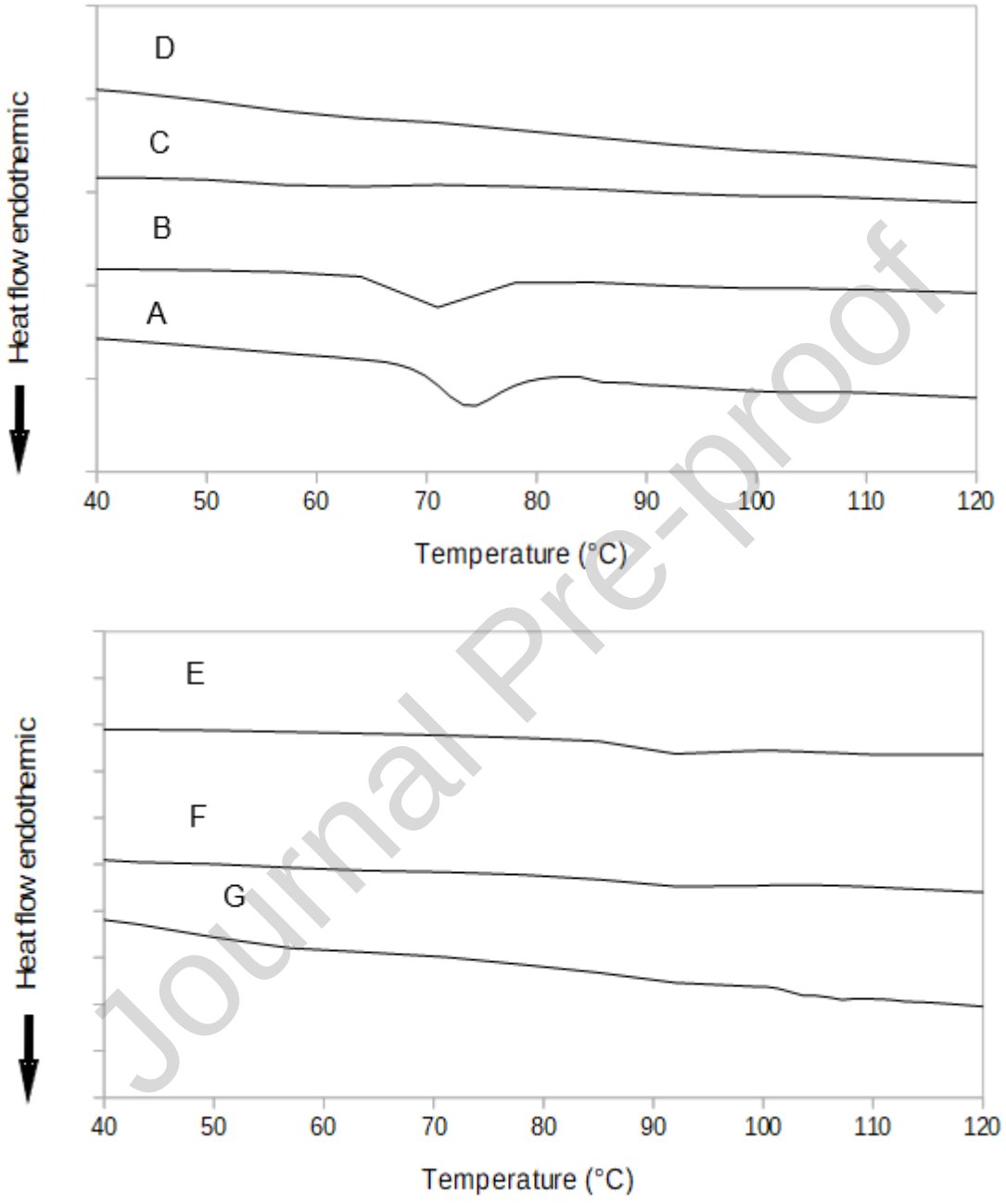

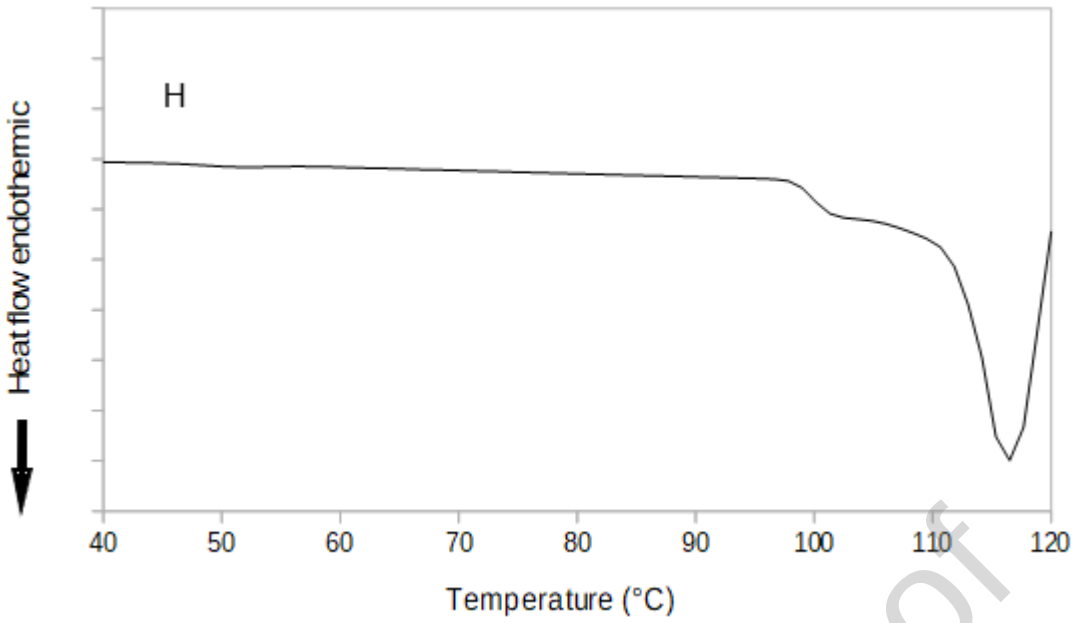

Figure 8. Thermograms of powders; **a)** unmilled starches: "A" (gelatinization) and "C" (retrogradation) for native corn starch, "B" (gelatinization) and "D" (retrogradation) for homogenized and spray-dried corn starch; **b)** corn starch powders obtained via WSMM: "E"for 7% (w/v) S + 1% (w/v) SDS, "F" for 7% (w/v) S + 0.07% (w/v) SDS, "G" for 7% (w/v) S; **c)** "H" for SDS.

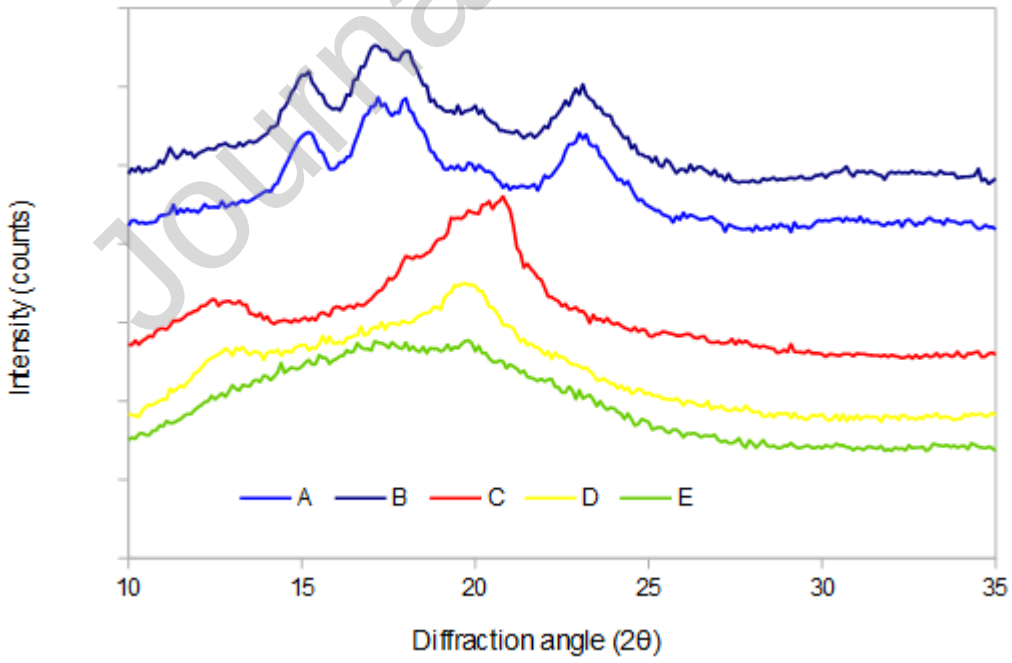

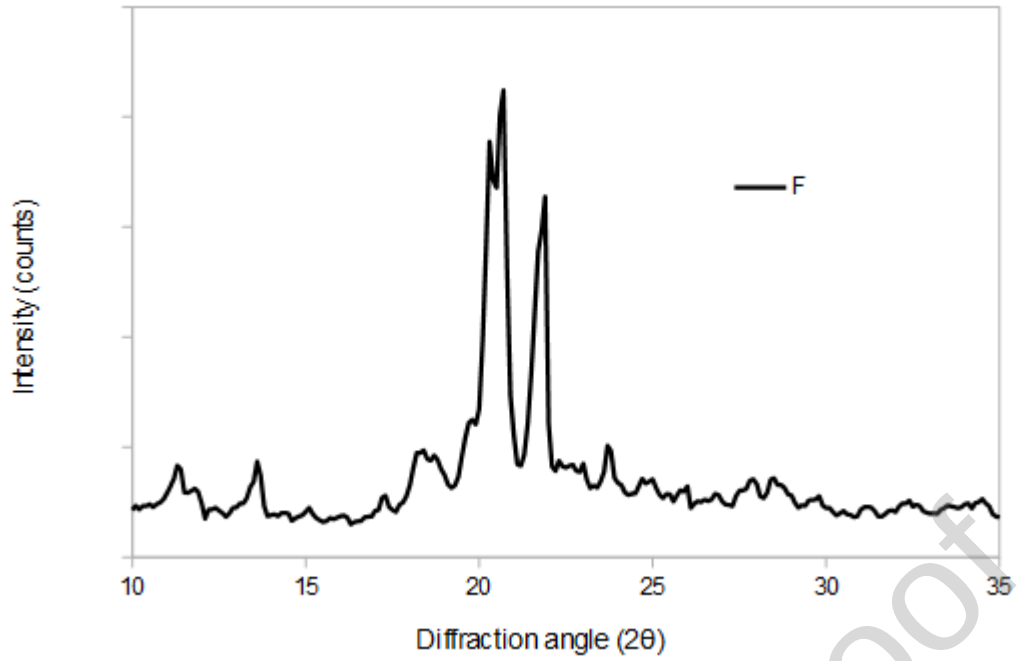

Figure 9. X-ray diffractograms of powders; **a)** starch samples: "A" (native corn starch), "B" (homogenized and spray-dried corn starch), and corn starch powders obtained via WSMM: "C" (7% (w/v) S, "D" (7% (w/v) S + 0.07% (w/v) SDS), "E" (7% (w/v) S + 1% (w/v) SDS); **b)** "F" (SDS).

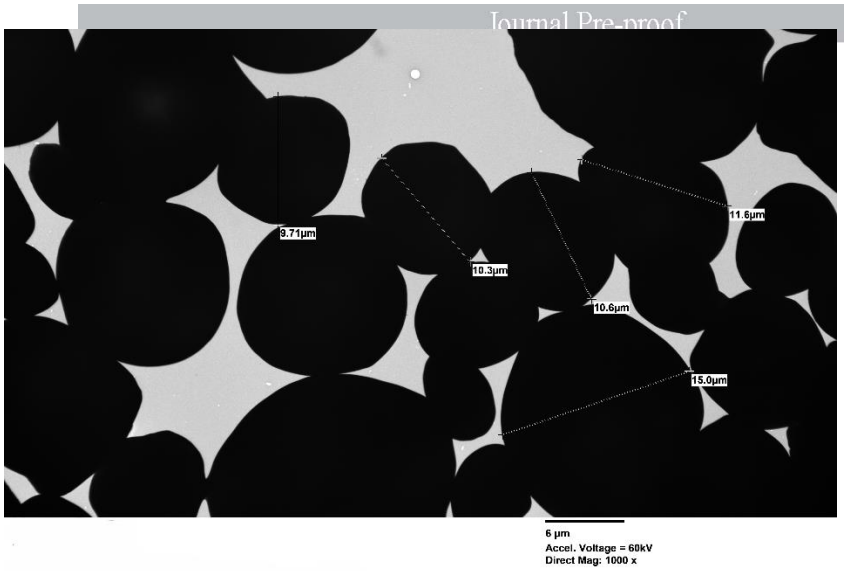

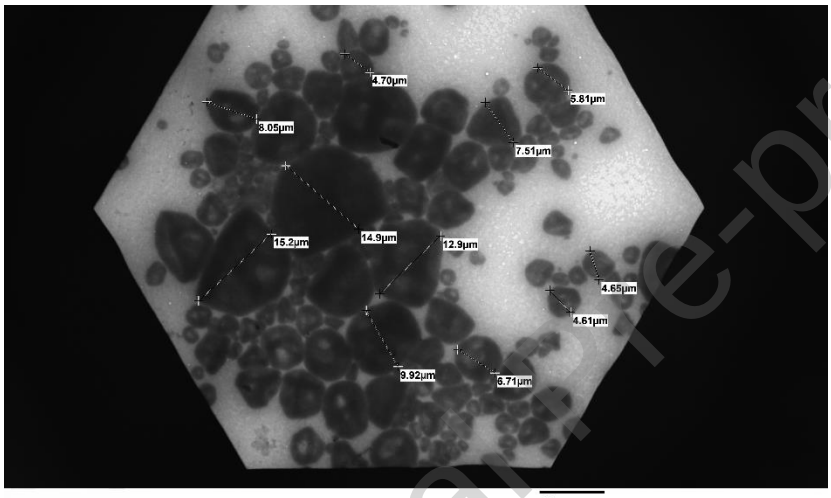

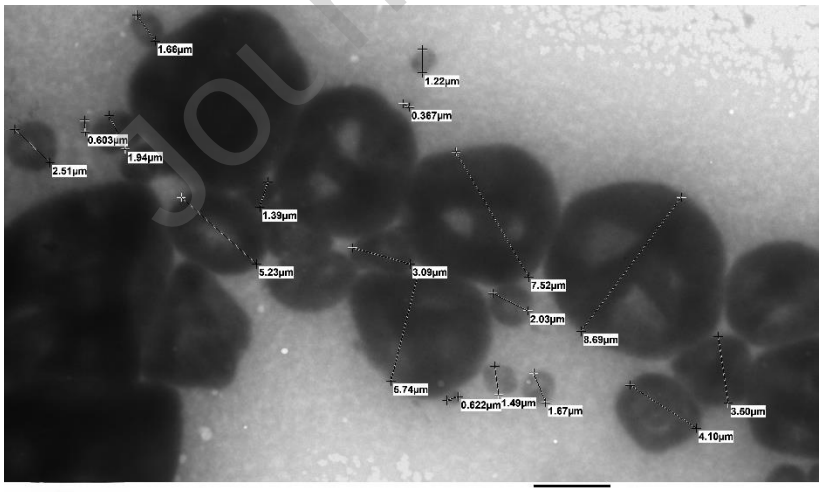

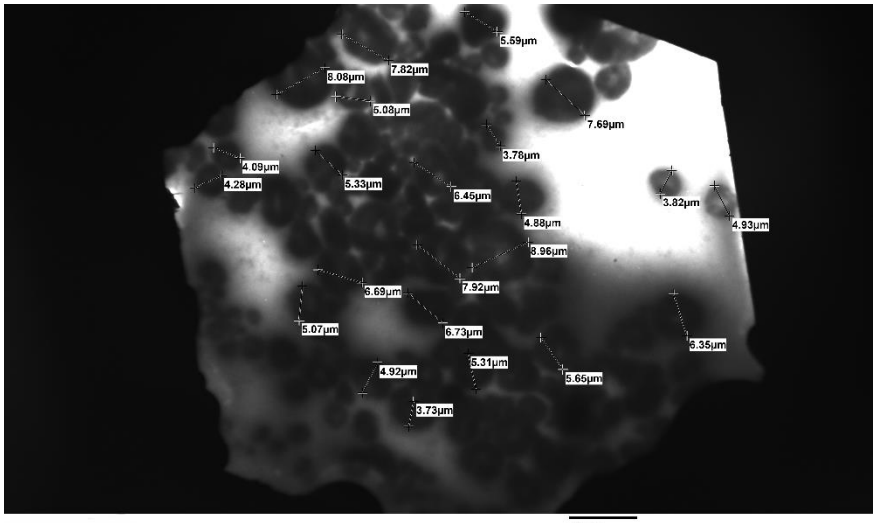

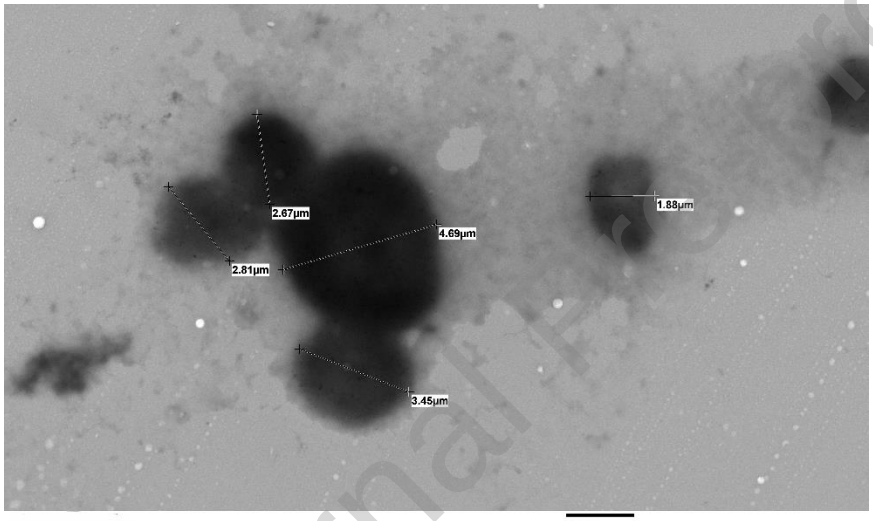

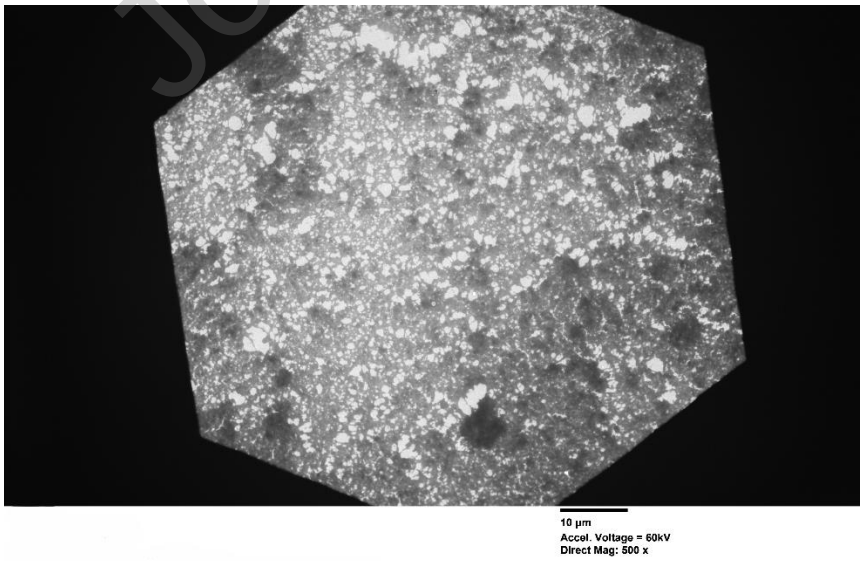

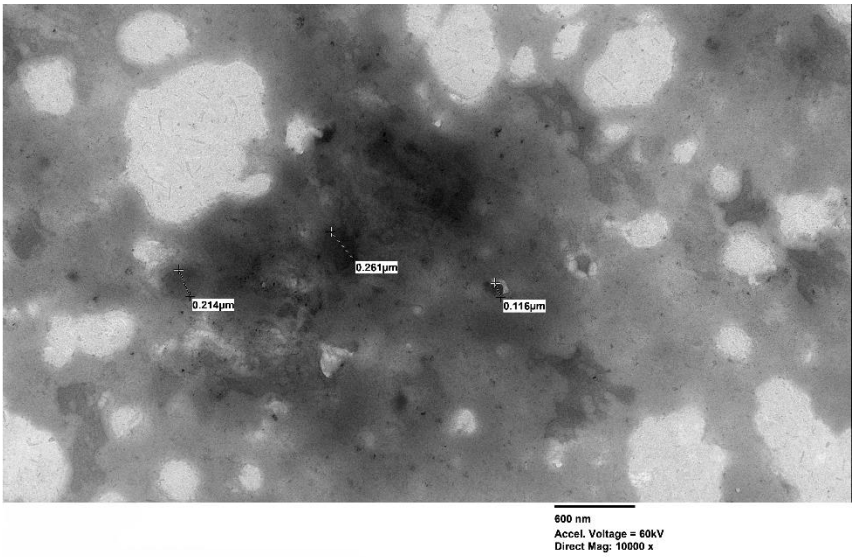

Figure 10. TEM micrographs of powders. Native corn starch: **a)** (500 x), **b)** (1000 x). Corn starch powders obtained via WSMM: 7% (w/v) S: **c)** (500 x), **d)** (1500 x); 7% (w/v) S + 0.07% (w/v) SDS: **e)** (500 x), **f)** (2500 x); 7% (w/v) S + 1% (w/v) SDS: **g)** (500 x), **h)** (10000 x).

Table 1. Preliminary experiments: particle size parameters (mean particle size and polydispersity index) and zeta potential of corn starch nanosuspensions

Starch concentration (% w/v)	*SDS concentration (% w/v)*	*Processing*	$Z_{av,0}$ (nm)	$Z_{av,f}$ (nm)	PDI_0	PDI_f	Zeta potential (mV)
1	-	M	416^{gh}±13	2194^{f}±121	0.33^{ef}±0.06	0.27^{ab}±0.08	-8.70^{ef}±0.26
		M + C	212^{c}±7	300^{bc}±8	0.23^{ab}±0.03	0.38^{de}±0.03	-7.68^{f}±0.28
		M +C + H	199^{e}±1	274^{e}±2	0.26^{a}±0.011	0.35^{f}±0.02	-9.23^{ef}±0.07
		M + H	315^{bc}±0	502^{bc}±4	0.18^{bc}±0.01	0.50^{cd}±0.08	-9.59^{ef}±0.95
1	0.01	M	444^{h}±2	416^{d}±2	0.31^{cde}±0.01	0.39^{de}±0.01	-16.70^{d}±1.80
		M + C	182^{ab}±2	182^{a}±1	0.24^{abc}±0.01	0.24^{a}±0.01	-12.43^{e}±0.60
		M +C + H	161^{f}±5	158^{c}±9	0.23^{efg}±0.12	0.22^{ab}±0.01	-19.00^{cd}±0.44

		M + H	373^{ab}±6	342^{a}±2	0.36^{ab}±0.06	0.27^{a}±0.01	–20.96^{c}±0.42
		M	397^{fg}±7	468de±9	0.40^{g}±0.03	0.44^{ef}±0.00	-62.26^{a}±5.39
		M + C	265^{d}±0	247^{b}±15	0.28^{bcd}±0.01	0.27^{ab}±0.09	-41.46^{b}±4.95
1	1	M +C + H	265^{d}±6	253^{c}±1	0.38^{fg}±0.01	0.33^{abc}±0.07	-39.40^{b}±2.19
		M + H	407^{d}±1	342^{b}±1	0.39^{efg}±0.01	0.29^{bcd}±0.03	-38.70^{b}±1.51

M: milling; C: centrifugation; H: homogenization; "0" and "f" subscripts are initial and final values after one week of storage, respectively; different letters in each column indicate statistically significant differences ($p<0.05$).

Table 2. Milling multilevel factorial design and response variables (particle size and zeta potential).

Starch concentration (% w/v)	SDS concentration (% w/v)	Bead diameter (mm)	$Z_{av,0}$ (nm)	$Z_{av,f}$ (nm)	$Z_{av,0,c}$ (nm)	$Z_{av,f,c}$ (nm)	PDI_0	PDI_f	$PDI_{0,c}$	$PDI_{f,c}$	Zeta potential (mV)
1	0.01	0.15	220.9^{a} ±12.4	290.75^{a} ±0.49	152.55^{b} ±12.80	151.25^{b}±0.07	0.35^{ab} ±0.05	0.44^{c} ±0.01	0.43^{b}± 0.11	0.36^{c}± 0.01	-12.9^{b}± 0.1
		0.50	206.25^{a}±0.07	301.0^{a} ±0.9	124.1^{a} ±1.4	124.2^{a} ±2.4	0.38^{b} ±0.05	0.45^{c} ±0.01	0.35^{ab} ±0.05	0.35^{bc} ±0.05	-11.15^{bc}±1.06
3.5	0.035	0.15	473.8^{d} ±13.3	466.9^{b}± 6.6	228.5^{d}± 5.6	224.55^{d}±0.35	0.17^{a} ±0.01	0.42^{c} ±0.01	0.29^{a}± 0.01	0.28^{a}± 0.01	-12.8^{b}± 1.3
		0.50	306.8^{b} ±2.1	307.0^{a} ±3.8	180.3^{c} ±0.8	175.7^{c} ±0.9	0.44^{b} ±0.01	0.36^{b} ±0.02	0.31^{ab} ±0.01	0.29^{ab} ±0.01	-14.75^{a} ±0.07
7	0.07	0.15	635.1^{e} ±23.6	765.6^{c}± 49.1	447.90^{f} ±13.65	439.45^{f}±3.46	0.71^{c} ±0.08	0.25^{a} ±0.01	0.29^{a}± 0.01	0.30^{ab} ±0.01	-17.20^{c} ±1.70
		0.50	431.4^{c} ±16.5	449.15^{b} ±10.39	288.73^{e} ±3.29	280.35^{e}±2.19	0.50^{b} ±0.14	0.56^{d} ±0.01	0.32^{ab} ±0.01	0.29^{abc} ±0.01	-19.73^{d} ±0.66

The improved SDS concentration as particle stabilizer was 1% w/w of the total starch concentration present in the formulation. Different letters in each column indicate statistically significant differences ($p<0.05$).

Table 3. Validation of the statistical model, under the optimal conditions

Response variable	Predicted value	Observed value	Error (%)
$Z_{av,0,c}$ (nm)	146.77	153.90±3.00	4.62
$Z_{av,f,c}$ (nm)	144.86	151.63± 1.00	4.47
$Z_{av,0}$ (nm)	279.26	313.87± 1.00	11.03
$Z_{av,f}$ (nm)	301.41	284.13±3.00	6.08
$PDI_{0,c}$	0.31	0.31± 0.03	0.08
$PDI_{f,c}$	0.31	0.27± 0.02	11.68
PDI_0	0.35	0.46± 0.01	23.35
PDI_f	0.42	0.31± 0.03	35.52
Zeta potential (mV)	-13.46	-19.03 ± 0.50	29.28

Table 4. Breakage kinetic constant for each milling condition

Starch concentration (% w/v)	SDS concentration (% w/v)	Bead diameter (mm)	k_m (s^{-1})	R^2
1	0.01	0.15	0.144 (0.010)	0.91
		0.50	0.308 (0.004)	0.97
3.5	0.035	0.15	0.119 (0.003)	0.89
		0.50	0.231 (0.010)	0.93
7	0.07	0.15	0.067 (0.010)	0.85
		0.50	0.133 (0.001)	0.99
2.48	0.0248	0.50	0.161 (0.010)	0.95

k_m values and their asymptotic standard errors between parenthesis are shown.

Table 5. Properties of parent nanosuspensions, and particle size of spray dried corn starch micro and nanoparticles

Starch concentration (% w/v)	SDS concentration (% w/v)	Bead diameter (mm)	$Z_{av,0}$ (nm)	ζ-potential (mV)	K ($Pa.s^n$)	n	$Z_{av,powder}$ (nm)	PDI_0	PDI_{powder}
7	-	0.15	$469.37^{a}\pm 7.64$	$-9.19^{a}\pm 0.16$	$0.003^{a}\pm 0.000$	$0.93^{a}\pm 0.00$	$9453.66^{c}\pm 239.60$	$0.31^{b}\pm 0.01$	$1.00^{b}\pm 0.00$
	0.07		$447.90^{a}\pm 13.65$	$-20.03^{b}\pm 0.47$	$0.002^{a}\pm 0.000$	$0.95^{a}\pm 0.01$	$5048.33^{b}\pm 541.03$	$0.25^{a}\pm 0.01$	$0.29^{a}\pm 0.01$
	1		$365.57^{b}\pm 2.98$	$-28.10^{c}\pm 0.53$	$0.006^{b}\pm 0.001$	$0.76^{b}\pm 0.05$	$271.06^{a}\pm 3.57$	$0.24^{a}\pm 0.01$	$0.27^{a}\pm 0.01$

Different letters indicate statistically significant differences ($p<0.05$).

Table 6. Thermal properties of native starch, and micro and nanoparticles

Formulation	Event	ΔH ($J.g^{-1}$)	T_o (°C)	T_p (°C)	T_e (°C)
NS	Gelatinization	$-10.61^{a}\pm 0.17$	$67.85^{a}\pm 0.56$	$73.10^{a}\pm 0.14$	$79.04^{a}\pm 0.06$
NS+H+S.D.	Gelatinization	$-11.13^{a}\pm 0.93$	$66.45^{a}\pm 0.51$	$72.22^{a}\pm 0.03$	$78.41^{a}\pm 0.01$
NS	Retrogradation	$-2.46^{a}\pm 0.23$	$51.75^{b}\pm 0.80$	$61.33^{b}\pm 2.33$	$67.68^{a}\pm 0.59$
NS+H+S.D.	Retrogradation	$-2.51^{a}\pm 0.35$	$48.97^{ab}\pm 2.18$	$59.62^{ab}\pm 0.00$	$71.03^{a}\pm 3.25$
7% (w/v) S	Retrogradation	$-0.79^{c}\pm 0.00$	$46.67^{a}\pm 0.00$	$57.48^{a}\pm 0.00$	$68.43^{a}\pm 3.25$
7% (w/v) S+0.07 % (w/v) SDS	Retrogradation	$-0.15^{b}\pm 0.00$	$50.14^{b}\pm 2.18$	$60.36^{ab}\pm 0.00$	$69.46^{a}\pm 0.00$
7% (w/v) S+0.07 % (w/v) SDS	Amylose-SDS complex dissociation	$-0.69^{a}\pm 0.00$	$87.57^{a}\pm 0.01$	$93.76^{a}\pm 0.00$	$99.26^{a}\pm 0.01$

7% (w/v) S+1 % (w/v) SDS	Amylose-SDS complex dissociation	-0.90[a]±0.00	84.63[a]±0.00	89.96[a]±0.01	93.42[a]±2.81

NS: native starch; H: homogenization; S.D.: spray drying; ΔH: enthalpy; T_o, T_p and T_e are the onset, peak and endset temperature, respectively. For each event type, different letters indicate statistically significant differences ($p<0.05$).

Declaration of interests

The authors declare that they have no known competing financial interests or personal relationships that could have appeared to influence the work reported in this paper.

Highlights

-Corn starch nanosuspensions were obtained via wet-stirred media milling (WSMM).

-The addition of SDS enhanced the physical stability of nanosuspensions.

-The use of larger zirconia beads yielded faster breakage kinetics.

-Larger beads and lower starch concentrations enhanced the microhydrodynamic parameters.

-Amylose-SDS complexes with improved emulsifying properties were formed.